A new thermodynamic model for clino- and orthoamphiboles in the system Na$_2$O–CaO–FeO–MgO–Al$_2$O$_3$–SiO$_2$–H$_2$O–O

J. F. A. DIENER,[1] R. POWELL,[1] R. W. WHITE[1]* AND T. J. B. HOLLAND[2]
[1]*School of Earth Sciences, The University of Melbourne, Melbourne, Vic. 3010, Australia (j.diener@pgrad.unimelb.edu.au)*
[2]*Department of Earth Sciences, University of Cambridge, Cambridge CB2 3EQ, UK*

ABSTRACT   A recent thermodynamic model for the Na–Ca clinoamphiboles in the system Na$_2$O–CaO–FeO–MgO–Al$_2$O$_3$–SiO$_2$–H$_2$O–O (NCFMASHO), is improved, and extended to include cummingtonite–grunerite and the orthoamphiboles, anthophyllite and gedrite. The clinoamphibole model in NCMASH is adopted, but the extension into the FeO- and Fe$_2$O$_3$-bearing systems is revised to provide thermodynamic consistency and better agreement with natural assemblage data. The new model involves order–disorder of Fe–Mg between the M2, M13 and M4 sites in the amphibole structure, calibrated using the experimental data on site distributions in cummingtonite–grunerite. In the independent set of end-members used to represent the thermodynamics, grunerite (rather than ferroactinolite) is used for FeO, with two ordered Fe–Mg end-members, and magnesioriebeckite (rather than ferritschermakite) is used for Fe$_2$O$_3$. Natural assemblage data for coexisting clinoamphiboles are used to constrain the interaction energies between the various amphibole end-members. For orthamphibole, the assumption is made that the site distributions and the non-ideal formulation is the same as for clinoamphibole. The data set end-members anthophyllite, ferroanthophyllite and gedrite, are used; for the others, they are based on the clinoamphibole end-members, with the necessary adjustments to their enthalpies constrained by natural assemblage data for coexisting clino- and orthoamphiboles. The efficacy of the models is illustrated with *P–T* grids and various pseudosections, with a particular emphasis on the prediction of mineral assemblages in ferric-bearing systems.

Key words: clinoamphibole; ferric iron; orthoamphibole; thermodynamics.

Mineral abbreviations: ab, albite; act, actinolite; anth, anthophyllite; chl, chlorite; cu, cummingtonite; di, diopside; ep, epidote; g, garnet; ged, gedrite; gl, glaucophane; hb, hornblende; hem, hematite; ilm, ilmenite; law, lawsonite; mt, magnetite; o, omphacite; pa, paragonite; pl, plagioclase; q, quartz; ru, rutile; sph, titanite.

INTRODUCTION

Prior to the publication of Dale *et al.* (2005), there had been no way of calculating mineral equilibria involving amphibole for geologically realistic systems (like Na$_2$O–CaO–FeO–MgO–Al$_2$O$_3$–SiO$_2$–H$_2$O–O, NCFMASHO) in which coexisting amphiboles could be considered with the same thermodynamic descriptions. For example, in Carson *et al.* (1999) and Wei *et al.* (2003), the descriptions of coexisting glaucophane and 'hornblende' (in this case, barroisitic amphibole) were written independently of each other. Although the calculated phase equilibria bore a reasonable similarity to the observed mineral assemblages, this is an incomplete and unsatisfactory approach to modelling minerals. Because glaucophane and hornblende share the same crystal structure, their descriptions should be identical, and the solvus between them should be a

consequence of that description. Not the least, the model should allow direct calculation of the closure of the solvus between these amphiboles without discontinuity, something that is obviously not going to be possible if the two amphiboles have different thermodynamic descriptions.

With the model in Dale *et al.* (2005), phase equilibria involving coexisting clinoamphiboles could be calculated for the first time. With the single thermodynamic description, the Na–Ca clinoamphibole in NCFMASHO at higher temperatures spans the compositional space, its solid solution only limited by the other minerals that are stable, and not by the solvi within the amphiboles themselves. On decreasing temperature, the interior part of the compositional space develops solvi, with the possibility of three-phase amphibole assemblages (e.g. Dale *et al.*, 2005, fig. 9). In metabasic rock compositions, such actinolite–hornblende–glaucophane-bearing assemblages can be developed in the vicinity of the greenschist–amphibolite–blueschist facies junction. At other pressures and temperatures, amphibole-bearing assemblages

Present address: Institute for Geosciences, University of Mainz, D-55099 Mainz, Germany.

commonly involve only one or two amphiboles, the others being excluded by the coexisting minerals (see Dale *et al.*, 2005 for the *sensu lato* naming convention used for amphibole).

The success of the Dale *et al.* (2005) model has been established in a series of recent papers (Štípská & Powell, 2005; Clarke *et al.*, 2006; Elmer *et al.*, 2006; Yang & Powell, 2006; Štípská *et al.*, 2006; Baldwin *et al.*, 2007) that involve calculated phase equilibria in primarily metabasic rock compositions. The current work was prompted by the need to extend the model to include cummingtonitic amphibole that has little Ca + Na on the amphibole M4 site, as well as orthoamphibole. On reappraisal of the Dale *et al.* (2005) model, it was concluded that amphibole more Fe-rich than that found in normal metabasic rocks was too ideal, and we aimed to correct this, while retaining the better-constrained, NCMASH, part of the model. We aimed also to improve the incorporation of ferric iron in the model. Additionally, Holland & Powell (2006) have shown that the equipartition assumption used in Dale *et al.* (2005), that

$$\left. Fe^{2+}/(Fe^{2+} + Mg) \right|_{M13} = \left. Fe^{2+}/(Fe^{2+} + Mg) \right|_{M2}$$
$$= \left. Fe^{2+}/(Fe^{2+} + Mg) \right|_{amph}$$

is thermodynamically inconsistent. The alternative, a full order–disorder model involving Fe–Mg partitioning between M2, M13 and M4, involves a prodigious number of extra interaction parameters, but some simple heuristics allowed these to be approximated. The remaining 'free' parameters in the thermodynamic description can be constrained using natural assemblage data for coexisting amphiboles, on recognition that such data provide the most powerful means of constraining non-ideality. This new amphibole model is outlined below, then various calculated phase diagrams are used to highlight phase equilibria using the model.

MODEL FORMULATION AND CALIBRATION OF THE CLINOAMPHIBOLES

Formulation

Model formulation follows that in Dale *et al.* (2005), except where explained here. Site occupancies in NCFMASHO adopted are as follows: in the one A site, Na and vacancy (□) may occur; in the three M13 sites, Mg and Fe^{2+}; in the two M2 sites, Al, Fe^{3+}, Mg and Fe^{2+}; in the two M4 sites, Ca, Na, Mg and Fe^{2+}; in the four T1 sites, Si and Al; in the four T2 sites, Si; and in the two hydroxyl sites, OH. Explicit Fe–Mg partitioning between the three types of octahedral sites (M4, M13 and M2) is modelled. An oxy-substitution involving the hydroxyl site is not considered and neither are constituents such as K, Ti and Mn. The amount of K and Ti in amphibole only becomes significant at granulite facies grades, which are currently outside of the

main application range in the blueschist, greenschist, epidote-amphibolite, amphibolite and eclogite facies. Using the above site distributions, an independent set of amphibole end-members within NCMASH is tremolite, tschermakite, pargasite, glaucophane and cummingtonite; adding FeO involves additionally grunerite, with end-members camo1 and camo2 to handle order–disorder (see below, and Holland & Powell, 2006), and adding Fe_2O_3, magnesioriebeckite:

End-member		Formula	A	M4	M13	M2	T1
Tremolite	tr	$Ca_2Mg_5Si_8O_{22}(OH)_2$	□	Ca_2	Mg_3	Mg_2	Si_4
Tschermakite	ts	$Ca_2Mg_3Al_2Si_6O_{22}(OH)_2$	□	Ca_2	Mg_3	Al_2	Al_2Si_2
Pargasite	parg	$NaCa_2Mg_4Al_3Si_6O_{22}(OH)_2$	Na	Ca_2	Mg_3	MgAl	Al_2Si_2
Glaucophane	gl	$Na_2Mg_3Al_2Si_8O_{22}(OH)_2$	□	Na_2	Mg_3	Al_2	Si_4
Cummingtonite	cumm	$Mg_2Mg_3Mg_2Si_8O_{22}(OH)_2$	□	Mg_2	Mg_3	Mg_2	Si_4
Grunerite	grun	$Fe_2Fe_3Fe_2Si_8O_{22}(OH)_2$	□	Fe_2	Fe_3	Fe_2	Si_4
Camo1	camo1	$Fe_2Mg_3Fe_2Si_8O_{22}(OH)_2$	□	Fe_2	Mg_3	Fe_2	Si_4
Camo2	camo2	$Fe_2Fe_3Mg_2Si_8O_{22}(OH)_2$	□	Fe_2	Fe_3	Mg_2	Si_4
Mg-riebeckite	mrb	$Na_2Mg_3Fe_2^{3+}Si_8O_{22}(OH)_2$	□	Na_2	Mg_3	Fe_2^{3+}	Si_4

An independent set of end-members allows a complete thermodynamic description of a phase:

$$G_{amph} = \sum_{i=1}^{n} p_i \left(G_i + RT \ln a_i^{ideal} + RT \ln \gamma_i \right) \quad (1)$$

in which G_{amph} is the Gibbs energy of the phase; G_i is the Gibbs energy of pure end-member, i; a_i^{ideal} is the ideal-mixing activity of end-member i; γ_i is the activity coefficient of i; p_i is the proportion of i; and n is the number of independent end-members in the phase. The ideal mixing activity is written in terms of ideal-mixing-on-sites, separately from the activity coefficient (e.g. Powell, 1977; Powell & Holland, 1993). The ideal-mixing activities used here are formulated in the same way as in Dale *et al.* (2005). The activity coefficients are written using the asymmetric formalism (Holland & Powell, 2003). This shares with the symmetric formalism (Powell & Holland, 1993) the property that the interactions are pairwise between the end-members in the independent set, with an interaction energy, W_{ij}, between each pair of end-members, i and j, with an asymmetry parameter, α_k, for each end-member k. The departure of $\alpha_i/(\alpha_i + \alpha_j)$ from 1/2 controls the degree of asymmetry in the i–j binary. The derivations of the corresponding interaction energies for other choices of the independent set, shown in Powell & Holland (1999) for the symmetric formalism, is given in Appendix 1 for the asymmetric formalism (correcting a logic error in the appendix of Dale *et al.* (2005), that nevertheless impacts little on the conclusions in that paper).

Calibration in FMSH

Following the approach in Holland & Powell (1996a,b), order–disorder in cummingtonite–grunerite clinoamphiboles is considered via two internal equilibria, $0 = -\Delta G^0 + RT \ln K$, for reactions between

cumm, grun and the two ordered end-members, camo1 and camo2 (corresponding to the end-members a and b in Holland & Powell, 1996b):

$$3\,\text{cumm} + 4\,\text{grun} = 7\,\text{camo1}$$
$$2\,\text{cumm} + 5\,\text{grun} = 7\,\text{camo2}. \tag{2}$$
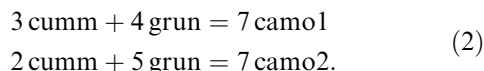
The site fractions and the proportions of the end-members can be written in terms of x, the macroscopic composition of the amphibole, $Fe^{2+}/(Fe^{2+} + Mg)|_{amph}$ and two order parameters, $Q_1 = x - Fe^{2+}/(Fe^{2+} + Mg)|_{M13}$ and $Q_2 = x - Fe^{2+}/(Fe^{2+} + Mg)|_{M2}$ (Q_1 and Q_2 are defined differently here than in Holland & Powell, 1996b). The unknowns are the two ΔH values (from the two ΔG^0) and the six macroscopic interaction energies, W_{ij}, pairwise between the four end-members. As emphasized in Holland & Powell (1996b), the experimentally determined site distribution data do not allow these eight unknowns to be constrained. The approach followed there was to assume that the x-dependent terms in the internal equilibria are zero, reducing the number of unknowns to six, then to resort to the microscopic equivalences of the macroscopic Ws (e.g. Powell & Holland, 1993), using a fixed value for Fe–Mg mixing on an octahedral site, and zero values for Fe–Mg cross-site mixing. This reduced the number of unknowns to be derived from the data to three, a number that the data can support, and this then provided the published calibration using the experimental data on site partitioning of Hirschmann et al. (1994).

A similar approach is followed here, with the macroscopic–microscopic equivalences written as

$$W_{\text{cumm grun}} = 7w_{\text{FeMg}} + 5w_{\text{FeFeMgMg}}$$
$$W_{\text{cumm camo1}} = 4w_{\text{FeMg}} + 2w_{\text{FeFeMgMg}}$$
$$W_{\text{cumm camo2}} = 5w_{\text{FeMg}} + 3w_{\text{FeFeMgMg}}$$
$$W_{\text{grun camo1}} = 3w_{\text{FeMg}} \tag{3}$$
$$W_{\text{grun camo2}} = 2w_{\text{FeMg}}$$
$$W_{\text{camo1 camo2}} = 5w_{\text{FeMg}}$$

with w_{FeMg} being the (microscopic) Fe–Mg interaction energy on an octahedral site, and w_{FeFeMgMg} being the cross-site Fe–Mg interaction energy between M13 and M4, and M2 and M4, with a zero cross-site term between the similar M13 and M2 sites assumed. Assuming that w_{FeMg} is the same as that for olivine, around 4 kJ mol^{-1} (e.g. Wiser & Wood, 1991), preliminary regression of the data suggested that w_{FeFeMgMg} is small and positive. Using a value of 1 kJ mol^{-1}, regression of the site distribution data gave

$$\Delta H_{\text{camo1}} = -66.2 \pm 2.7\,\text{kJ mol}^{-1}$$
$$\Delta H_{\text{camo2}} = -81.2 \pm 2.1\,\text{kJ mol}^{-1} \tag{4}$$

for the two reactions in Eq. (2), with $W_{\text{cumm grun}} = 33$, $W_{\text{cumm camo1}} = 18$, $W_{\text{cumm camo2}} = 23$, $W_{\text{grun camo1}} = 12$, $W_{\text{grun camo2}} = 8$, and $W_{\text{camo1 camo2}} = 20$ (in
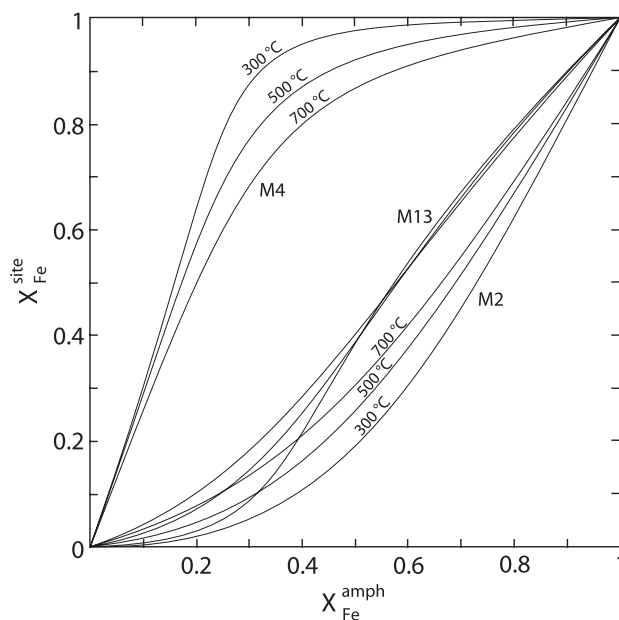
Fig. 1. Calculated partitioning of Fe and Mg onto M13, M2 and M4 sites in cummingtonite as a function of $x = X_{\text{Fe}}^{\text{amph}}$ at 300, 500 and 700 °C.

kJ mol^{-1}) and with $\alpha = 1$ for these end-members. The calculated partitioning of Mg and Fe in the cummingtonite structure is shown in Fig. 1 and shows excellent agreement with other published models (e.g. fig. 2 of Evans & Ghiorso, 1995; Holland & Powell, 1996b). Small changes to the assumptions will cause the fit parameters to change – for example, if w_{FeMg} for M4 is made somewhat smaller as this is a larger site – but the quality of the fit is most unlikely to be affected, and its effect on the rest of the model will be minimal.

Calibration in CFMSH

The addition of CaO involves the consideration of tremolite, tr. Continuing with the macroscopic–microscopic equivalences

$$W_{\text{tr cumm}} = 2w_{\text{CaMg}}^{\text{M4}}$$
$$W_{\text{tr grun}} = 2w_{\text{CaFe}}^{\text{M4}} + 5w_{\text{FeMg}} + 5w_{\text{FeFeMgCa}}$$
$$W_{\text{tr camo1}} = 2w_{\text{CaFe}}^{\text{M4}} + 2w_{\text{FeMg}} + 2w_{\text{FeFeMgCa}} \tag{5}$$
$$W_{\text{tr camo2}} = 2w_{\text{CaFe}}^{\text{M4}} + 3w_{\text{FeMg}} + 3w_{\text{FeFeMgCa}}$$

with w_{FeFeMgCa} being a cross-site term that is assumed to be the same for M13–M4 and M2–M4 mixing. Following Dale et al. (2005), progress in calibration requires making analogies between non-ideality in Fe end-member and Mg end-member amphiboles using dependent end-member equivalences (Powell & Holland, 1999). In Dale et al. (2005), it was assumed that Fe end-member amphiboles were rather more ideal than Mg end-member amphiboles, but it is now con-

sidered that the case for this was not well made. Considerable uncertainty exists with respect to the relative idealities of the Fe and Mg subsystems and the shape of amphibole solvi as Fe–Mg changes. Whereas the natural data of Ghiorso & Evans (2002) and experimental data of Jenkins & Bozhilov (2003) suggest that the Fe subsystem amphiboles are more ideal than their magnesian counterparts, the natural data of Spear (1980) and experimental data of Oba & Nicholls (1986) contradict this and suggest that the Fe subsystem might be less ideal than the Mg one. The natural data for both clino- and orthoamphiboles compiled during this study (Tables 1 & 2) do not suggest that there are major differences in non-ideality between the Fe and Mg subsystems. Considering the lack of definitive data, it is assumed here that the Fe subsystem and Mg subsystem amphiboles have similar non-ideality; so, for example, w_{CaFe}^{M4} is taken to equal w_{CaMg}^{M4}.

Calibration of the two resulting unknowns, w_{CaMg}^{M4} and $w_{FeFeMgCa}$, was made with reference to the size and shape of the Ca-amphibole–cummingtonite solvus in relation to natural assemblage data (Table 1 & Fig. 2). The experiments of Cameron (1975) as well as natural data suggest that the solvus may be slightly asymmetric, with a steeper cummingtonite limb, so that α_{cumm} would be slightly less than α_{tr}. However, here we chose to keep the solvus symmetric as, given the scatter of the data, the degree of asymmetry is hard to quantify (Ghiorso & Evans, 2002, fig. 2). From the natural assemblage data in Fig. 2, the unknowns were constrained to be $2w_{CaMg}^{M4} = 45\,kJ\,mol^{-1}$ and $w_{FeFeMgCa} = 2\,kJ\,mol^{-1}$. This then gives (in $kJ\,mol^{-1}$):

$W_{i,j}$	tr	cumm	grun	camo1	camo2
tr		45	75	57	63
cumm			33	18	23
grun				12	8
camo1					20
α_i	1	1	1	1	1

Calibration in CFMSH allows calculation of the cation ordering in actinolite. Mitchell *et al.* (1970) and Evans & Yang (1998) have shown that, in contrast to the pronounced Fe–Mg ordering exhibited by cummingtonite (Fig. 1), ordering in the calcic amphiboles is much weaker and the distribution of Fe and Mg in the tremolite–ferroactinolite series is essentially disordered. These studies only considered Fe–Mg partitioning between M1, M2 and M3 in the actinolite structure and could not resolve Fe–Mg partitioning onto M4, as this site is almost completely occupied by Ca. Recently, Driscall *et al.* (2005) investigated the M4 partitioning in synthetic low-Ca actinolite and found that actinolite exhibits a strong preferential partitioning of Fe onto M4 that is even more pronounced than in cummingtonite. Calculation of site distributions for

actinolite (Fig. 3) agree very well with these data and show that the partitioning of Fe and Mg onto M2 and M13 is much weaker than for cummingtonite (Fig. 1), whereas the partitioning of Fe onto M4 is more pronounced.

Calibration in NCMASH

The interaction energies and asymmetry parameters are adopted from Dale *et al.* (2005) with the exception of a slight decrease of $W_{tr\,parg}$, to reflect the change in the relative non-ideality of the Fe and Mg end-member systems (see above), and the rounding up of $W_{ts\,parg}$. So now the resulting interaction parameters (in $kJ\,mol^{-1}$) are:

$W_{i,j}$	tr	ts	parg	gl
tr		20	25	65
ts			−40	25
parg				50
α_i	1.0	1.5	1.7	0.8

Calibration in NCFMASH

Assuming that the Fe end-member and Mg end-member amphiboles have similar non-ideality, as already adopted above, allows the extension from NCMASH to NCFMASH. Using the above values for the interaction energies, the remaining values are provided by the dependent end-member constraints, bar one unconstrained value (refer to Appendix 3 for details of the dependent end-member constraints). This value was constrained by the natural assemblage data involving coexisting hornblende and cummingtonite (Figs 4 & 5), giving (in $kJ\,mol^{-1}$):

$W_{i,j}$	tr	ts	parg	gl	cumm	grun	camo1	camo2
tr		20	25	65	45	75	57	63
ts			−40	25	70	80	70	72.5
parg				50	90	106.7	94.8	94.8
gl					100	113.5	100	111.2
cumm						33	18	23
grun							12	8
camo1								20
α_i	1	1.5	1.7	0.8	1	1	1	1

As mentioned above, the assumption that the NCMASH and NCFASH subsystems have the same non-ideality is a significant departure from the model of Dale *et al.* (2005). This is illustrated in Fig. 6, which can be directly compared with fig. 5c and f of Dale *et al.* (2005). A notable feature of the hornblende–actinolite solvus, when plotted as a function of $x = Fe/(Fe + Mg)$ is that, whereas the width is the same in the

Table 1. Natural data of coexisting hornblende and cummingtonite.

Reference	Sample	T (°C)	P (kbar)	Hornblende						Cummingtonite					
				x	y	z	a	c	f	x	y	z	a	c	f
1	17 2	580	6	0.352	0.357	0.028	0.423	0.865	0.055	0.372	0.008	0.014	0	0.072	0.051
1	17 4	580	6	0.353	0.36	0.035	0.385	0.862	0.053	0.385	0	0	0	0.065	0.053
2	ID 7-4	550	5	0.755	0.347	0.005	0.314	0.963	0.071	0.717	0	0	0.039	0.053	0.099
2	IW 809-1J	550	5	0.655	0.225	0.021	0.239	0.859	0.142	0.647	0	0.017	0.022	0.072	0.088
3	14	670	4	0.564	0.393	0.031	0.461	0.791	0.154	0.494	0.016	0.03	0.092	0.123	0.19
3	4C	670	4	0.809	0.168	0.013	0.411	0.893	0.131	0.797	0.015	0.001	0.003	0.067	0.007
3	1A	670	4	0.722	0.124	0.009	0.095	0.907	0.295	0.749	0.022	0	0	0.073	0.002
3	13A	670	4	0.78	0.201	0.016	0.186	0.898	0.15	0.803	0.035	0.015	0.002	0.1	0.004
4	1317	550	5	0.394	0.458	0.002	0.029	0.717	0.033	0.357	0.028	0.001	0.001	0.062	0.07
5	70	685	6	0.51	0.343	0.049	0.296	0.764	0.08	0.497	0.087	0.035	0.046	0.165	0.07
5	76	655	6	0.485	0.316	0.068	0.27	0.851	0.043	0.478	0.042	0.012	0.017	0.095	0.026
5	74a	660	6	0.571	0.287	0.033	0.512	0.785	0.098	0.515	0.012	0.023	0.053	0.1	0.125
5	82	680	6	0.249	0.25	0.078	0.176	0.802	0.048	0.309	0.051	0.013	0.014	0.093	0.022
5	65a	630	6	0.355	0.275	0.036	0.366	0.773	0.099	0.348	0.013	0.017	0.033	0.097	0.106
5	67	685	6	0.421	0.356	0.027	0.306	0.752	0.141	0.401	0.086	0.026	0.053	0.11	0.102
6	6A	700	5	0.6	0.179	0.013	0.149	0.895	0.148	0.606	0	0	0.024	0.06	0.084
6	SL48	700	5	0.63	0.179	0.039	0.224	0.892	0.061	0.664	0	0	0	0.054	0.093
6	9E	700	5	0.683	0.195	0.019	0.272	0.845	0.123	0.668	0	0	0.021	0.069	0.09
6	9K	700	5	0.681	0.199	0.015	0.242	0.885	0.204	0.707	0	0	0	0.029	0.097
6	SL69	700	5	0.577	0.223	0.013	0.147	0.847	0.182	0.606	0	0.008	0.019	0.053	0.083
6	G2	700	5	0.62	0.209	0.013	0.3	0.91	0.322	0.605	0.044	0.004	0	0.051	0.082
6	G3	700	5	0.504	0.131	0.015	0.168	0.875	0.28	0.524	0	0	0.003	0.056	0.072
6	P3	400	3	0.542	0.125	0.024	0.272	0.817	0.245	0.588	0.009	0.006	0	0.069	0.079
6	P1	400	3	0.43	0.206	0.023	0.308	0.839	0.207	0.426	0.027	0	0	0.117	0.083
7	W4	625	4.5	0.376	0.4	0.022	0.438	0.85	0.216	0.356	0.01	0.019	0.043	0.133	0.109
7	W19	625	4.5	0.535	0.403	0.021	0.313	0.875	0.225	0.507	0.055	0.005	0.01	0.068	0.031
8	W-2b	610	6	0.464	0.514	0.043	0.491	0.815	0.084	0.402	0.051	0.008	0.015	0.085	0.038
9	12	530	6.5	0.535	0.428	0.055	0.506	0.825	0.07	0.455	0.016	0.01	0	0.036	0.064
10	QB27c2a	650	6	0.326	0.423	0.027	0.306	0.773	0.164	0.345	0.099	0.014	0	0.109	0.046
10	QB27c2b	650	6	0.347	0.598	0.043	0.3	0.771	0.074	0.341	0.113	0.014	0	0.109	0.045
11	2a	625	5.5	0.347	0.598	0.043	0.3	0.771	0.074	0.341	0.113	0.014	0	0.109	0.045
11	2b	625	5.5	0.326	0.423	0.027	0.306	0.773	0.164	0.345	0.099	0.014	0	0.109	0.046
12	7b	600	8	0.554	0.375	0.018	0.432	0.891	0.159	0.473	0	0.017	0	0.038	0.066
12	8	600	8	0.55	0.414	0.018	0.396	0.881	0.091	0.48	0.004	0.02	0	0.042	0.066
12	9c	600	8	0.611	0.405	0.021	0.469	0.863	0.226	0.521	0.011	0.046	0	0.033	0.071
12	9d	600	8	0.566	0.42	0.023	0.513	0.853	0.17	0.49	0	0.007	0.014	0.034	0.068
12	10b	600	8	0.629	0.46	0.016	0.488	0.892	0.054	0.523	0.002	0.02	0.056	0.049	0.01
12	11b	600	8	0.625	0.43	0.018	0.469	0.872	0.153	0.525	0	0	0	0.036	0.073
12	11c	600	8	0.43	0.427	0.019	0.393	0.864	0.118	0.394	0	0	0	0.055	0.055
13	73-20D	535	5.5	0.538	0.544	0.036	0.426	0.805	0.079	0.437	0.023	0.011	0.021	0.032	0.091
13	73-30I	535	5.5	0.394	0.607	0.097	0.315	0.799	0.059	0.375	0.012	0.003	0	0.039	0.053
13	77-56C	535	5.5	0.408	0.554	0.049	0.389	0.8	0.078	0.357	0.018	0.003	0	0.042	0.05
14	73-30N	535	5.5	0.404	0.639	0.106	0.326	0.812	0.047	0.366	0.023	0.003	0	0.036	0.051
14	73-30S	535	5.5	0.422	0.588	0.087	0.342	0.813	0.06	0.408	0	0.002	0.002	0.042	0.058
14	73-25C	535	5.5	0.531	0.609	0.056	0.385	0.812	0.068	0.431	0.026	0.007	0	0.035	0.06
14	73-20C	535	5.5	0.542	0.555	0.051	0.471	0.801	0.078	0.449	0.053	0.026	0	0.04	0.062
14	73-19D	535	5.5	0.3	0.436	0.021	0.426	0.863	0.148	0.326	0.013	0.01	0	0.055	0.045
14	77-57	535	5.5	0.392	0.5	0.036	0.423	0.814	0.084	0.349	0.031	0.015	0	0.046	0.048
15	100	700	8.6	0.244	0.225	0.005	0.392	0.956	0.257	0.307	0	0	0	0.055	0.043
15	103	700	8.6	0.117	0.125	0.015	0.419	0.782	0.207	0.212	0	0	0	0.051	0.03
16	F3	650	3.5	0.398	0.166	0.025	0.284	0.832	0.085	0.463	0.013	0.034	0	0.086	0.063
16	F68	650	3.5	0.204	0.292	0.031	0.313	0.809	0.08	0.265	0.022	0	0	0.077	0.073
16	F33	650	3.5	0.59	0.2	0.014	0.465	0.879	0.145	0.575	0.059	0.065	0	0.139	0.072
17	101A	550	5	0.461	0.558	0.064	0.502	0.815	0.064	0.393	0.044	0.015	0.028	0.047	0.042
17	Gab1	550	5	0.424	0.54	0.018	0.304	0.902	0.046	0.383	0.039	0	0	0.055	0.053
17	Gab2	550	5	0.225	0.357	0.021	0.289	0.862	0.154	0.333	0.023	0.01	0.008	0.085	0.012

$x = Fe^{2+}/(Fe^{2+} + Mg)$; $y = X_{Al}^{M2}$; $z = X_{Na}^{M4}$; $a = X_{Na}^{A}$; $c = X_{Ca}^{M4}$; $f = X_{Fe3+}^{M2}$. Details of the recalculation procedure are given in Appendix 2. 1 = Brady (1974); 2 = Dymek & Klein (1988); 3 = Gole & Klein (1981); 4 = Hawthorne *et al.* (1980); 5 = Hollocher (1991); 6 = Immega & Klein (1976); 7 = James *et al.* (1978); 8 = Kahl & Schumacher (2000); 9 = Miyake (1984); 10 = Robinson & Jaffe (1969); 11 = Robinson *et al.* (1969); 12 = Sampson & Fawcett (1977); 13 = Spear (1980); 14 = Spear (1982); 15 = Srikantappa *et al.* (1985); 16 = Stephenson & Hensel (1979); 17 = Stout (1972).

Mg and Fe subsystems, it decreases to a minimum at $x = 0.6$. This minimum is an unexpected consequence of the partitioning of Fe and Mg between the M4, M13 and M2 sites in the amphibole structure. With increasing temperature, the solvus first closes at the intermediate x value of 0.6, while remaining open in more Mg-rich and Fe-rich compositions (Fig. 6d). Because the vast majority of mafic rocks are relatively magnesian (with $x < 0.6$), applying the model to 'normal' compositions will make it appear that it is moderately more ideal for Fe-rich compositions.

Calibration in NCFMASHO

Whereas Dale *et al.* (2005) considered ferric iron in terms of a ferritschermakite end-member, here it is

Table 2. Natural data of coexisting gedrite and anthophyllite.

Reference	Sample	T (°C)	P (kbar)	Gedrite						Anthophyllite					
				x	*y*	*z*	*a*	*c*	*f*	*x*	*y*	*z*	*a*	*c*	*f*
1	17d-71	550	5	0.504	0.424	0.044	0.231	0.024	0.062	0.447	0.104	0.024	0.037	0.016	0.056
2	1	450	2.5	0.88	0.915	0.003	0.504	0.011	0.051	0.728	0.025	0	0	0	0.102
2	2	450	2.5	0.821	0.739	0.008	0.328	0.001	0.15	0.699	0.037	0.016	0.031	0.006	0.159
3	14	530	6.5	0.369	0.399	0.052	0.243	0.048	0.066	0.338	0.101	0.022	0.004	0.028	0.006
4	OR-26A	575	3	0.58	0.459	0.025	0.312	0.016	0.178	0.503	0.011	0.014	0	0.01	0.071
4	OR-27D	575	3	0.541	0.512	0.028	0.436	0.011	0.088	0.458	0.056	0.038	0.075	0.019	0.148
4	OR-40C	575	3	0.571	0.428	0.022	0.247	0.04	0.148	0.511	0.08	0.002	0.004	0.002	0.052
4	PN-3C	575	3	0.453	0.509	0.024	0.433	0.034	0.147	0.337	0.078	0.07	0.14	0.031	0.304
4	218-B	575	3	0.324	0.394	0.033	0.378	0.016	0.148	0.296	0.029	0.042	0.083	0.011	0.207
5	73-20D	535	5.5	0.539	0.512	0.029	0.497	0.037	0.088	0.436	0.04	0.008	0.017	0.022	0.066
5	68-432U	535	5.5	0.316	0.533	0.098	0.258	0.026	0.07	0.292	0.177	0.045	0.012	0.023	0.019
5	68-432D	535	5.5	0.27	0.518	0.077	0.219	0.018	0.059	0.255	0.102	0.016	0.013	0.008	0.02
6	73-20C	535	5.5	0.521	0.483	0.067	0.439	0.034	0.093	0.449	0.109	0.035	0.013	0.02	0.02
6	73-30I	535	5.5	0.42	0.519	0.078	0.313	0.037	0.085	0.374	0.082	0.017	0.022	0.027	0.034
6	73-30N	535	5.5	0.424	0.558	0.086	0.362	0.044	0.079	0.37	0.062	0.018	0	0.025	0.051
6	73-30S	535	5.5	0.455	0.491	0.094	0.283	0.05	0.076	0.391	0.071	0.02	0	0.028	0.054
6	73-56C	535	5.5	0.406	0.499	0.06	0.302	0.052	0.082	0.362	0.102	0.017	0.001	0.028	0.002
6	73-57	535	5.5	0.383	0.4	0.028	0.393	0.046	0.204	0.332	0.09	0.033	0.067	0.032	0.132
6	73-58D	535	5.5	0.323	0.389	0.047	0.319	0.045	0.086	0.293	0.154	0.035	0.018	0.029	0.027
6	68-432M	535	5.5	0.367	0.54	0.11	0.281	0.039	0.076	0.331	0.159	0.048	0.019	0.03	0.029
6	73-37N	535	5.5	0.387	0.614	0.047	0.288	0.034	0.069	0.35	0.109	0.019	0.018	0.028	0.028
6	68-432J	535	5.5	0.283	0.421	0.033	0.386	0.03	0.118	0.262	0.063	0.024	0.047	0.016	0.123
7	GE2	550	5	0.41	0.32	0.022	0.244	0.016	0.176	0.417	0.217	0.028	0.03	0.008	0.047
7	101A	550	5	0.394	0.314	0.035	0.414	0.055	0.212	0.383	0.104	0.034	0.046	0.024	0.07
7	101AB	550	5	0.385	0.319	0.031	0.447	0.063	0.255	0.385	0.108	0.03	0.052	0.023	0.081
7	161A	550	5	0.315	0.337	0.025	0.288	0.047	0.123	0.268	0.001	0.002	0.053	0.023	0.134

$x = Fe^{2+}/(Fe^{2+} + Mg)$; $y = X^{M2}_{Al}$; $z = X^{M4}_{Na}$; $a = X^A_{Na}$; $c = X^{M4}_{Ca}$; $f = X^{M2}_{Fe3+}$. Details of the recalculation procedure are given in Appendix 2. 1 = Clark (1978); 2 = Frimmel (1996); 3 = Miyake (1984); 4 = Schneiderman & Tracy (1991); 5 = Spear (1980); 6 = Spear (1982); 7 = Stout (1972).

done by the addition of magnesioriebeckite. This is considered to be a more useful approach because of the strong affinity of glaucophane for Fe^{3+}. By analogy with jadeite–acmite pyroxene (Popp & Gilbert, 1972; Liu & Bohlen, 1995) and grossular–andradite garnet (Holdaway, 1972), the model assumes the same non-ideality for the Fe^{3+}-free and Al-free subsystems and allows complete solid solution between glaucophane and magnesioriebeckite ($W_{gl\ mrb} = 0$ and $\alpha_{gl} = \alpha_{mrb}$). The interaction energies between magnesioriebeckite and all other end-members are assumed to be the same as for glaucophane. The model calibration in the full NCFMASHO system then becomes (in kJ mol^{-1}):

$W_{i,j}$	tr	ts	parg	gl	cumm	grun	camo1	camo2	mrb
tr		20	25	65	45	75	57	63	65
ts			-40	25	70	80	70	72.5	25
parg				50	90	106.7	94.8	94.8	50
gl					100	113.5	100	111.2	0
cumm						33	18	23	100
grun							12	8	113.5
camo1								20	100
camo2									111.2
α_i	1	1.5	1.7	0.8	1	1	1	1	0.8

The provision of complete solid solution between the NCFMASH and NCFMSHO subsystems is another deviation from the model of Dale *et al.* (2005), which considered the ferric-bearing system to be more ideal

than the ferric-free system. This is illustrated in Figs 7 & 8, using the data of Dale *et al.* (2005) for coexisting actinolite and glaucophane (Fig. 8 provides a direct comparison with fig. 7c and f of Dale *et al.*, 2005). Most of the natural data are relatively low in ferric iron, with $Fe^{3+}/(Fe^{3+} + Al) < 0.2$ (Fig. 7a), while glaucophane is enriched in ferric iron relative to actinolite (Fig. 8a). However, the partitioning of Fe^{3+} and Al are very similar for both actinolite and glaucophane at low ferric contents but the data become more scattered with increasing ferric iron (Fig. 7a). The model is able to reproduce these features at low ferric contents, and then extrapolate them to the Al-free system (Figs 7b & 8b).

FORMULATION AND CALIBRATION OF THE ORTHOAMPHIBOLES

Formulation

The formulation of the orthoamphibole model follows that of clinoamphibole and considers the same components and exchange vectors. The chosen independent set of end-members in NCMASH is anthophyllite and gedrite and the fictive end-members orthomagnesiopargasite, orthoglaucophane and orthotremolite. Expansion to include FeO involves the addition of ferroanthophyllite and the ordered end-members amo1 and amo2, while including Fe_2O_3 adds the fictive orthomagnesioriebeckite end-member.

End-member		Formula	A	M4	M13	M2	T1
Anthophyllite	anth	$Mg_2Mg_5Si_8O_{22}(OH)_2$	□	Mg_2	Mg_3	Mg_2	Si_4
Gedrite	ged	$Mg_2Mg_3Al_4Si_6O_{22}(OH)_2$	□	Mg_2	Mg_3	Al_2	Al_2Si_2
Ortho-Mg-pargasite	ompa	$NaMg_2Mg_4Al_3Si_6O_{22}(OH)_2$	Na	Mg_2	Mg_3	$MgAl$	Al_2Si_2
Orthoglaucophane	omgl	$Na_2Mg_3Al_2Si_8O_{22}(OH)_2$	□	Na_2	Mg_3	Al_2	Si_4
Orthotremolite	otr	$Ca_2Mg_3Mg_2Si_8O_{22}(OH)_2$	□	Ca_2	Mg_3	Mg_2	Si_4
Ferroanthophyllite	fanth	$Fe_2Fe_3Fe_2Si_8O_{22}(OH)_2$	□	Fe_2	Fe_3	Fe_2	Si_4
Amo1	amo1	$Fe_2Mg_3Fe_2Si_8O_{22}(OH)_2$	□	Fe_2	Mg_3	Fe_2	Si_4
Amo2	amo2	$Fe_2Fe_3Mg_2Si_8O_{22}(OH)_2$	□	Fe_2	Fe_3	Mg_2	Si_4
Ortho-Mg-riebeckite	omrb	$Na_2Mg_3Fe_2^{3+}Si_8O_{22}(OH)_2$	□	Na_2	Mg_3	Fe_2^{3+}	Si_4

(a)

(b)
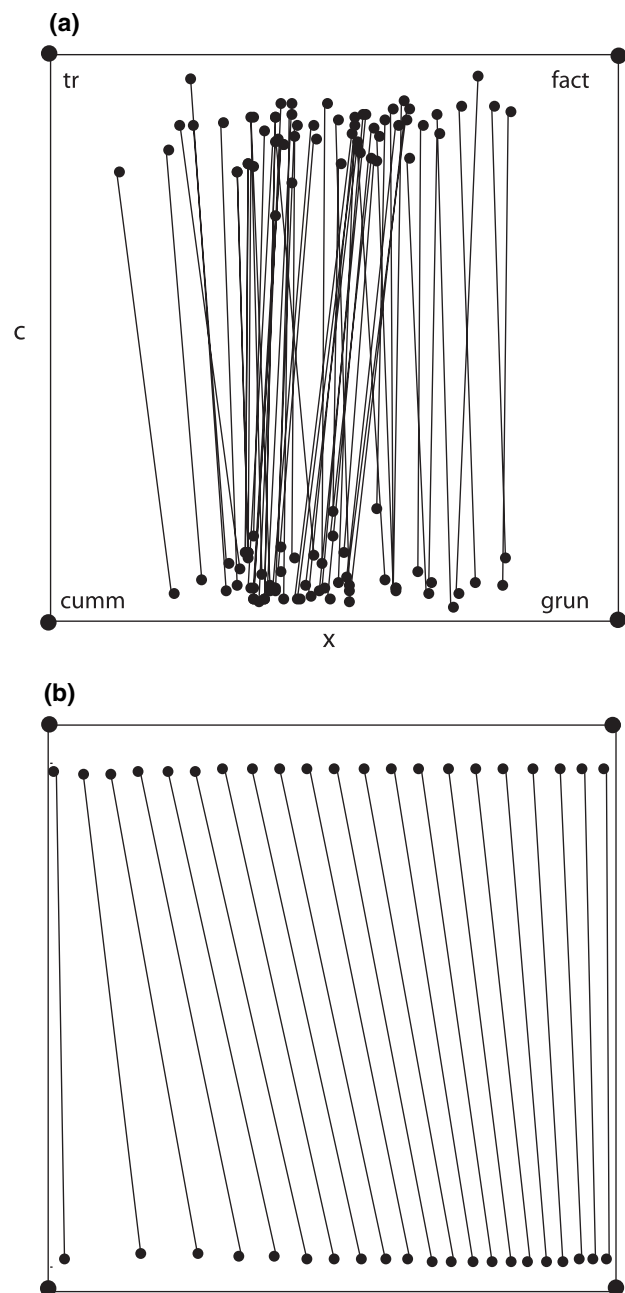
Fig. 2. Comparison of (a) observed and (b) modelled coexisting Ca-amphibole and cummingtonite in CFMSH at 600 °C. Data represented in terms of variations in $x = X_{Fe}^{amph}$ and $c = X_{Ca}^{M4}$.
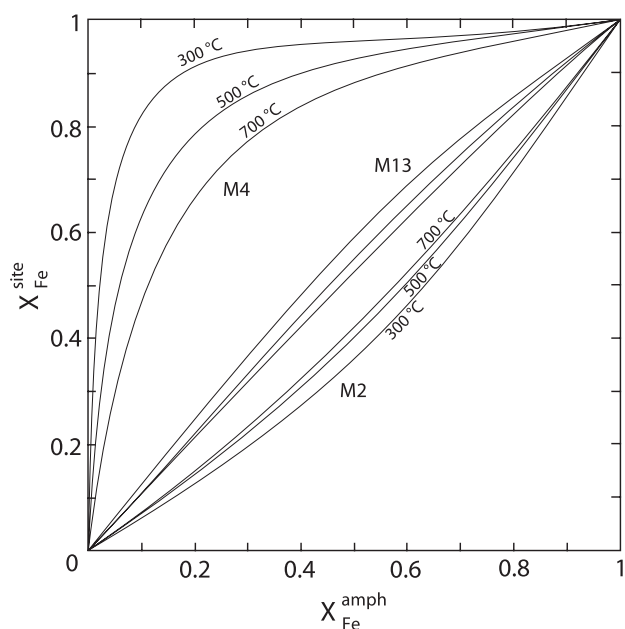
Fig. 3. Calculated partitioning of Fe and Mg onto M13, M2 and M4 sites in actinolite as a function of $x = X_{Fe}^{amph}$ at 300, 500 and 700 °C.

Calibration in FMSH and CFMSH

Considering the similarity between the anthophyllite–ferroanthophyllite and cummingtonite–grunerite series, it is reasonable to assume that the ordering of Fe and Mg in anthophyllite–ferroanthophyllite is identical to that in cummingtonite–grunerite (Evans *et al.*, 2001). Additionally, the amount of CaO accommodated in the anthophyllite structure is similar (albeit slightly lower) than that in cummingtonite (Robinson *et al.*, 1982; Ghiorso & Evans, 2002). This suggests that the anthophyllite–orthotremolite solvus has a similar size and shape as that between cummingtonite and actinolite. The simplest approach to calibration is to assume that the orthoamphiboles have the same non-ideality as the clinoamphiboles in CFMSH, and to address the slight difference in CaO content by adjustments to the end-member thermodynamic properties (see below). The orthoamphibole calibration in CFMSH is (in kJ mol^{-1}):

$W_{i,j}$	otr	anth	fanth	amo1	amo2
otr		45	75	57	63
anth			33	18	23
fanth				12	8
amo1					20
α_i	1	1	1	1	1

Calibration in NCMASH

Natural data of coexisting anthophyllite and gedrite (Table 2 & Fig. 9) show that the orthoamphibole
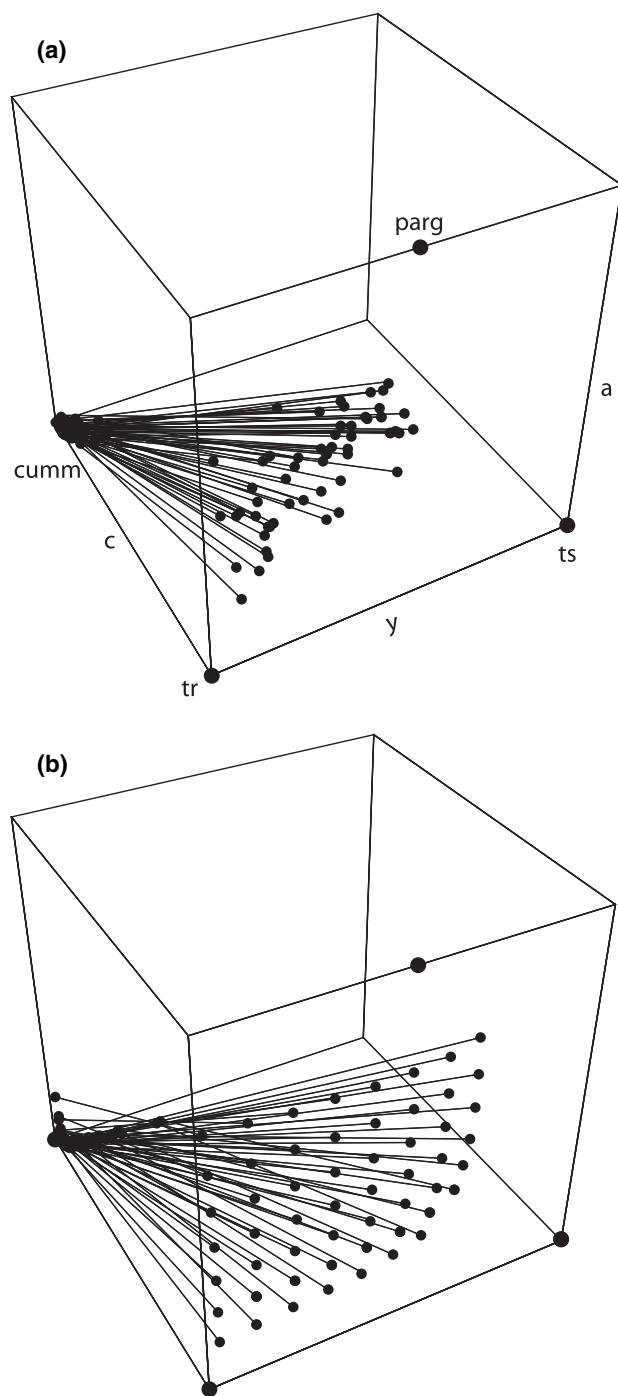
(a)

(b)

Fig. 4. Three-dimensional representation of (a) observed and (b) modelled coexisting Ca-amphibole and cummingtonite in NCMASH at 600 °C. Data represented in terms of variations in $y = X^{M2}_{Al}$, $a = X^A_{Na}$ and $c = X^{M4}_{Ca}$.

solvus is analogous to that between hornblende and actinolite (Robinson *et al.*, 1971; Spear, 1980). This suggests that the interaction energies and asymmetry parameters of the orthoamphiboles are very similar to those of the clinoamphiboles in NCMASH. As a first approximation these are assumed to be the same, with

the exception of $W_{\text{anth ged}}$, which is taken as 25 kJ mol^{-1} (instead of 20 kJ mol^{-1}) to place the top of the orthoamphibole solvus at just over 600 °C, as this appears to match the natural data more closely (Fig. 10; Spear, 1980, 1982; Robinson *et al.*, 1982). Minor differences between the ortho- and clinoamphiboles, such as differences in the amount of X^A_{Na} in gedrite and hornblende, are handled by adjustments to the end-member thermodynamic properties (see below). The NCMASH calibration for orthoamphibole is (in kJ mol^{-1}):

$W_{i,j}$	anth	ged	ompa	omgl
anth		25	25	65
ged			-40	25
ompa				50
α_i	1.0	1.5	1.7	0.8

Calibration in NCFMASH and NCFMASHO

The extension of the orthoamphibole model to include FeO follows the same procedure as for the clinoamphiboles, assuming that mixing in the Fe and Mg subsystems have the same non-ideality, with one unconstrained value that was calibrated using natural assemblage data involving coexisting anthophyllite and gedrite. The incorporation of ferric iron is also handled in the same way as for the clinoamphiboles, so that the complete orthoamphibole NCFMASHO calibration is (in kJ mol^{-1}):

$W_{i,j}$	anth	ged	ompa	omgl	otr	fanth	amo1	amo2	omrb
anth		25	25	65	45	33	18	23	65
ged			-40	25	70	38.5	29	34.6	25
ompa				50	90	45	33.2	36	50
omgl					65	81.2	65.5	78.4	0
otr						75	57	63	65
fanth							12	8	81.2
amo1								20	65.5
amo2									78.4
α_i	1	1.5	1.7	0.8	1	1	1	1	0.8

It has been demonstrated by Papike & Ross (1970), Seifert & Virgo (1975) and Seifert (1978) that the degree of Fe–Mg ordering in the orthoamphibole structure is dependent on the amount of Al in the orthoamphibole as well as temperature. The distribution of Fe and Mg in orthoamphibole becomes less ordered with increasing Al content, so that the ordering in gedrite is less pronounced than anthophyllite. The degree of ordering in low-Al anthophyllite also decreases rapidly with increasing temperature, but this effect is much less pronounced in aluminous gedrite (Papike & Ross, 1970; Seifert & Virgo, 1975; Seifert, 1978). Calculation of site distributions for anthophyllite and gedrite (Fig. 11) agree with these data and show that the partitioning of Fe and Mg between M4
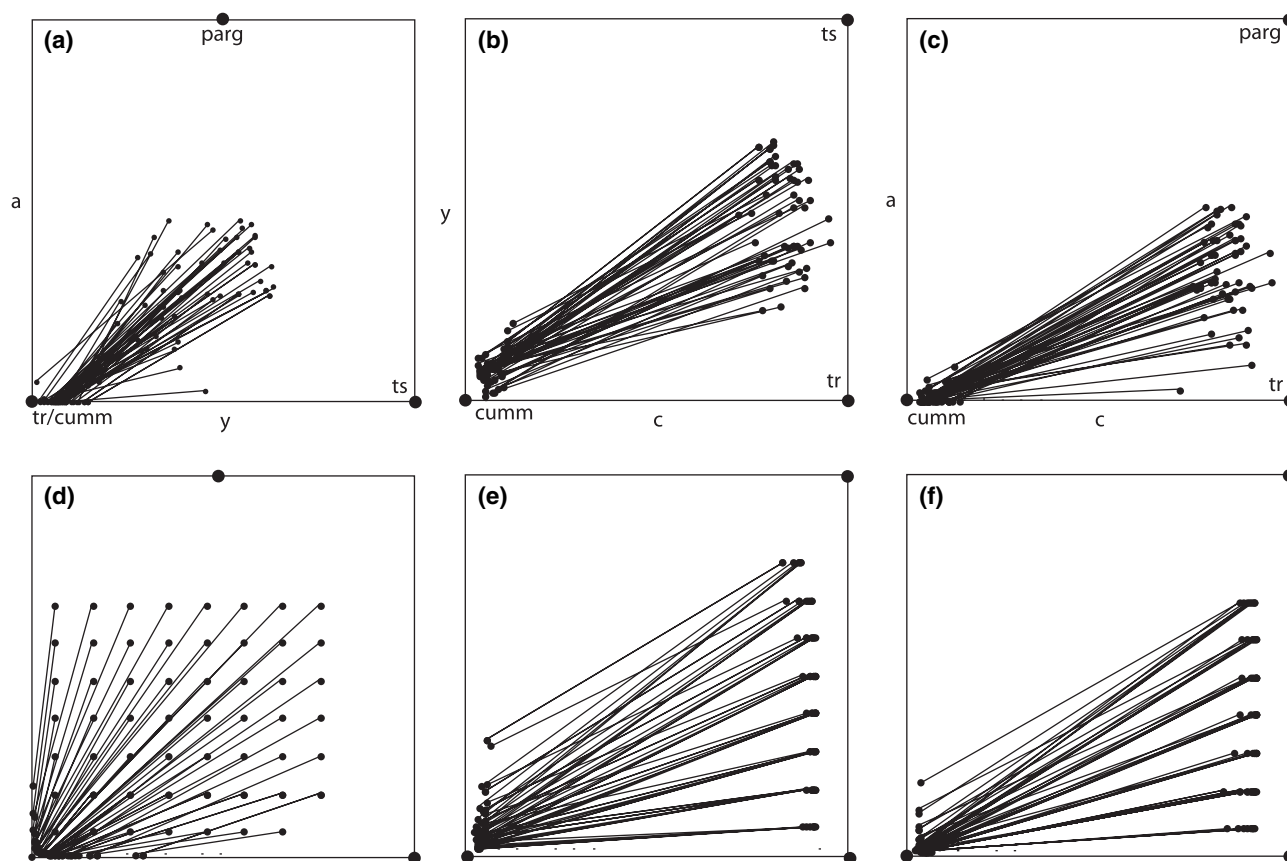
Fig. 5. Two-dimensional representations of the data presented in Fig. 4. (a,d): viewed along the *c*-axis in terms of $y = X_{Al}^{M2}$ and $a = X_{Na}^{A}$; (b,e): viewed along the *a*-axis in terms of $c = X_{Ca}^{M4}$ and *y*; (c,f): viewed along the *y*-axis in terms of *c* and *a*.

and M13 is more pronounced in anthophyllite and weakens with increasing Al content. Partitioning is also strongly dependent on temperature in anthophyllite, but is almost independent of temperature in aluminous gedrite (Fig. 11).

Summary of predictions in NCFMASHO

The development of models for both the clino- and orthoamphiboles allows calculations to be made for the first time in this geologically realistic system and provides a capacity to predict the compositions of coexisting ortho- and clinoamphiboles. These assemblages are known to occur in nature, with the most spectacular examples containing four coexisting amphiboles (hornblende, cummingtonite, anthophyllite and gedrite). The Telemark area in Norway (Stout, 1971, 1972) and the Post Pond Volcanics of Vermont (Spear, 1980, 1982) are two well-known localities where four-amphibole assemblages have been described. Data from these localities are presented in Tables 1 & 2 and the relationships between the coexisting phases are shown in Fig. 12. Calculations in the full NCFMASHO system predict the coexistence of these four amphiboles and agree very well with the natural data (Fig. 12).

CALIBRATION OF THERMODYNAMIC END-MEMBER DATA

Up to this point, the calibration involved only the *a–x* relations that constrain the size and shape of amphibole solvi but does not provide any constraints on the stability of the amphiboles with respect to other phases. To fix the *a–x* calibration in *P–T* space, the thermodynamic properties of other phases in NCFMASHO as well as the properties of the amphibole end-members need to be assessed. Whereas the properties of certain amphibole end-members are well known from experimental data, the properties of other end-members are less well constrained and require evaluation in light of the new *a–x* model and possibly adjustment to agree with natural data. In addition, the thermodynamic properties of end-members that are not in the internally consistent data set of Holland & Powell (1998) must be constrained. Following the logic of Holland & Powell (1998), enthalpies – being the least well established of the thermodynamic properties – are the data that are adjusted.

The fictive end-members are made by a linear combination of end-members that are in the thermodynamic data set, and their enthalpies have to be adjusted by a value, δ_i, relative to that of their constituents:
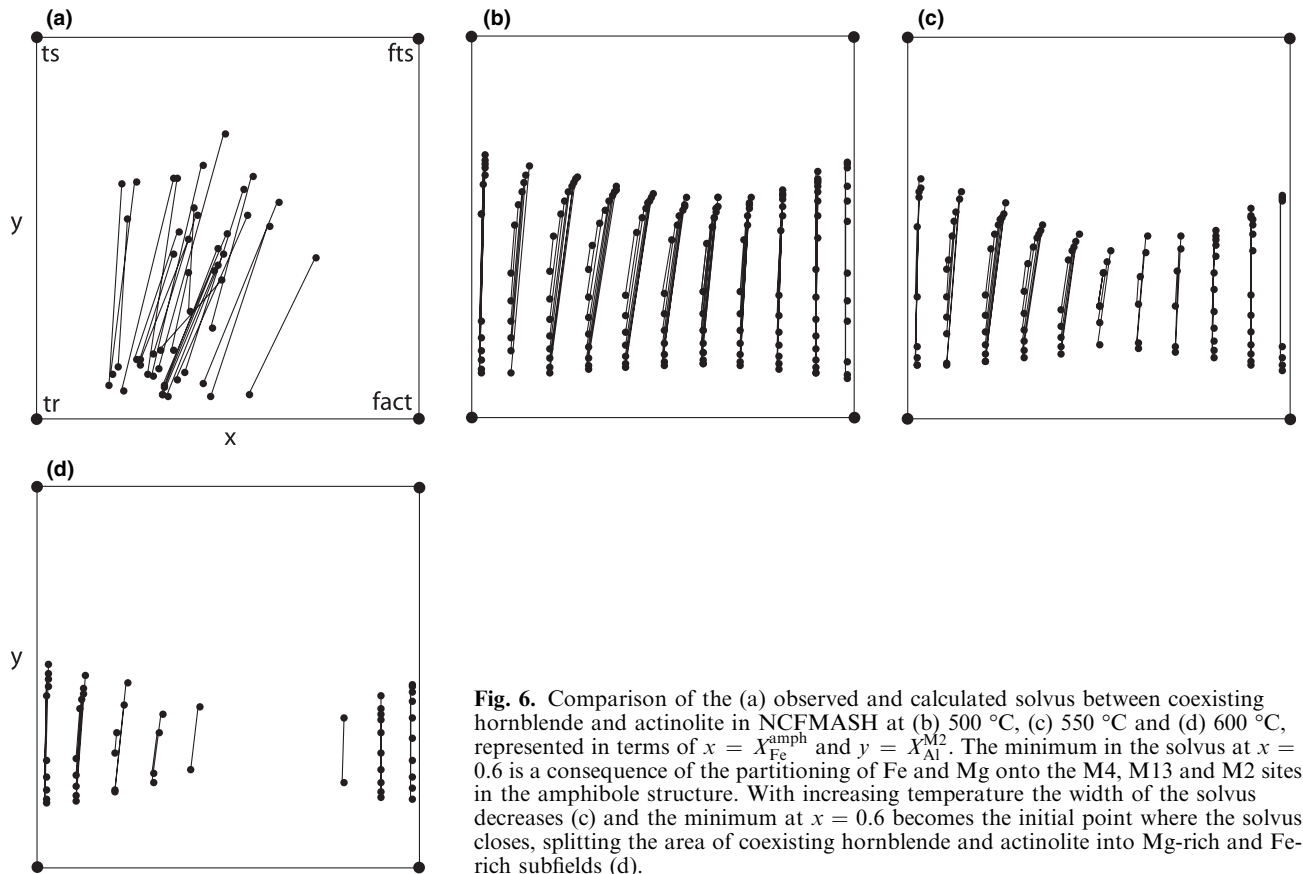
Fig. 6. Comparison of the (a) observed and calculated solvus between coexisting hornblende and actinolite in NCFMASH at (b) 500 °C, (c) 550 °C and (d) 600 °C, represented in terms of $x = X_{Fe}^{amph}$ and $y = X_{Al}^{M2}$. The minimum in the solvus at $x = 0.6$ is a consequence of the partitioning of Fe and Mg onto the M4, M13 and M2 sites in the amphibole structure. With increasing temperature the width of the solvus decreases (c) and the minimum at $x = 0.6$ becomes the initial point where the solvus closes, splitting the area of coexisting hornblende and actinolite into Mg-rich and Fe-rich subfields (d).

$$\Delta_f H_{mrb} = \Delta_f H_{gl} - 2\Delta_f H_{jadeite} + 2\Delta_f H_{acmite} + \delta_{mrb}$$
$$\Delta_f H_{ompa} = \Delta_f H_{parg} - \Delta_f H_{tr} + \Delta_f H_{anth} + \delta_{ompa}$$
$$\Delta_f H_{omgl} = \Delta_f H_{gl} + \delta_{omgl}$$
$$\Delta_f H_{otr} = \Delta_f H_{tr} + \delta_{otr}$$
$$\Delta_f H_{omrb} = \Delta_f H_{gl} - 2\Delta_f H_{jadeite} + 2\Delta_f H_{acmite} + \delta_{omrb}.$$

$$(6)$$

In the following, we use natural data to constrain enthalpy adjustments as experimental data are commonly incapable of achieving the precision required to, for example, represent the relative stability of the amphibole polymorphs (Evans *et al.*, 2001). Calculated pseudosections are used in comparison with well-known natural examples because they have the necessary sensitivity to the end-member properties to allow these properties to be constrained.

Thermodynamic properties in FMSH

Here we follow the approach of Evans *et al.* (2001), who showed that the temperature of the anthophyllite–cummingtonite transition is dependent on $x = Fe/(Fe + Mg)$, providing a strong constraint on the thermodynamic properties of the FMSH end-members. Anthophyllite and cummingtonite are known to coexist in amphibolites with $x \approx 0.3$ at 550 °C and

metaperidotites with $x \approx 0.1$ at 650 °C (Evans *et al.*, 2001). This provides the position and slope of the anthophyllite–cummingtonite transition in *P–T–x*. Assuming that the thermodynamic end-member properties for anthophyllite are well constrained by experimental data (Holland & Powell, 1998), the properties of cummingtonite, grunerite and ferro-anthophyllite were adjusted to fit these data (Fig. 13). From this, it is concluded that the $\Delta_f H$ of cummingtonite has to be adjusted by -6.4 kJ mol^{-1}, grunerite by -5 kJ mol^{-1} and ferroanthophyllite by 7 kJ mol^{-1} relative to the values in Holland & Powell (1998).

Whereas there is good agreement between this calibration and that of Evans *et al.* (2001) over the range of x that encompasses the natural data (Fig. 13), they begin to diverge at $x > 0.5$, with the calibration of Evans *et al.* (2001) displaying a minimum in the cummingtonite–anthophyllite transition at $x \approx 0.7$. The minimum was introduced by Evans & Ghiorso (1995, fig. 3) in relation to data for Al in natural orthoamphibole that was not explicitly included in their model. As the model presented here does explicitly account for Al, and, considering a lack of definitive natural data for the minimum, we did not attempt to reproduce it. Even if the minimum should be there, it would not affect the application of the model in all but the most Fe-rich compositions.
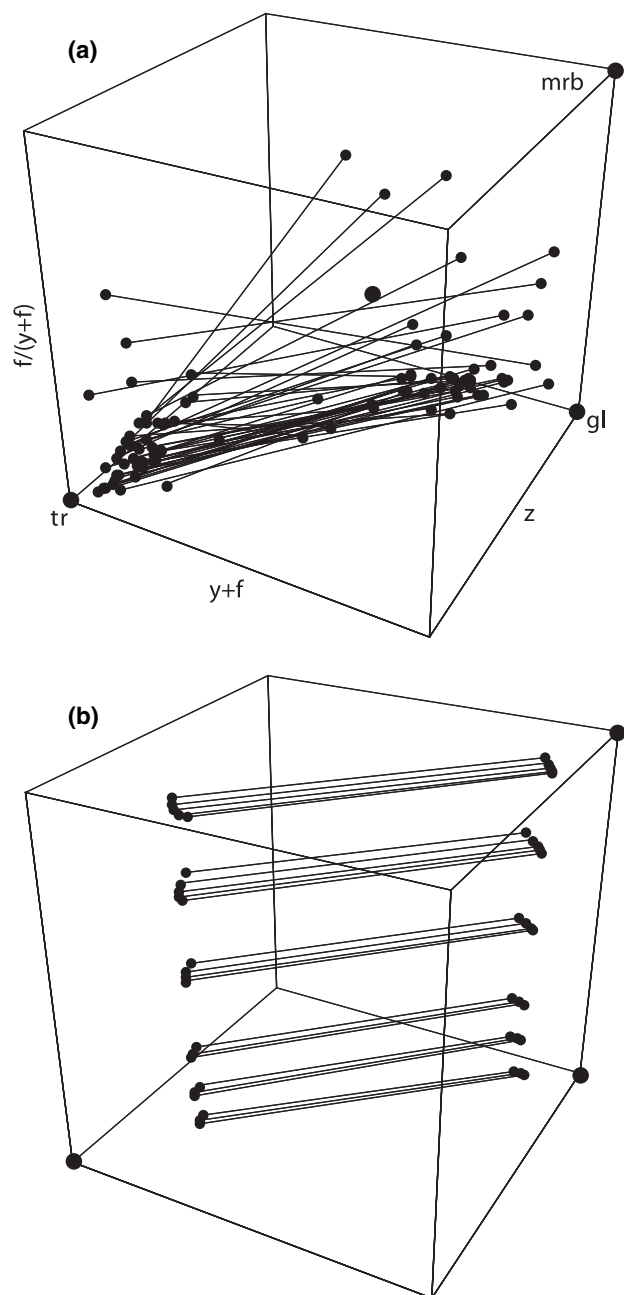
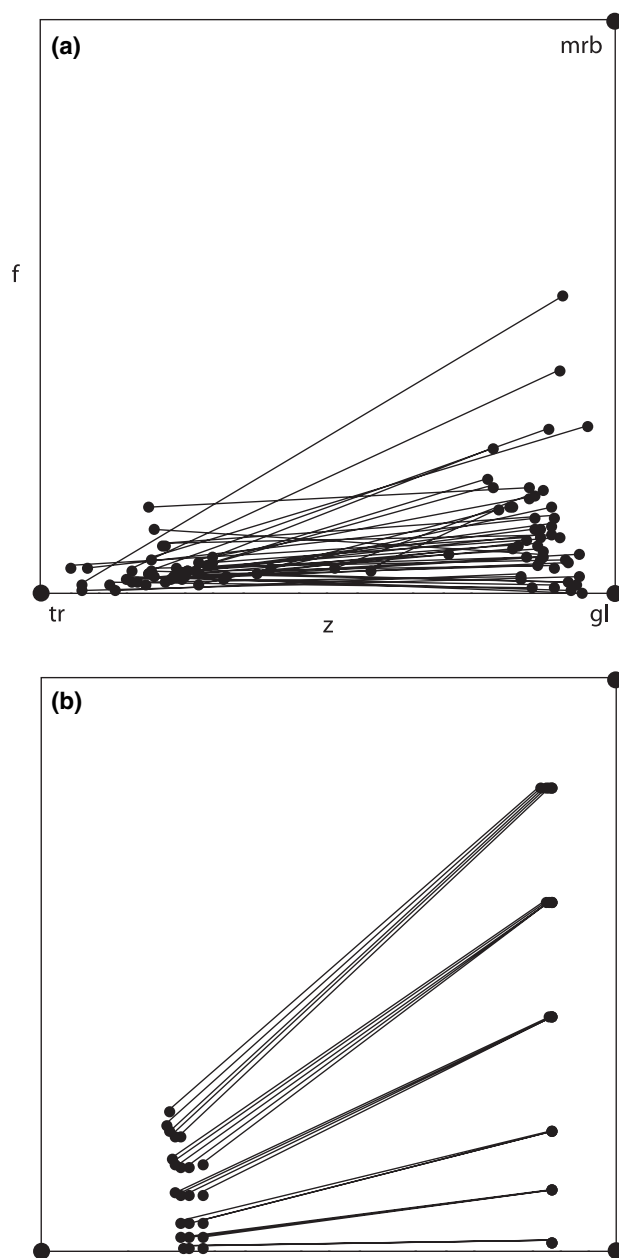**Fig. 7.** Three-dimensional representation of (a) observed and (b) calculated coexisting actinolite and glaucophane in NCFMASHO at 500 °C. Data are represented in terms of variations in $y + f = X_{Al}^{M2} + X_{Fe3+}^{M2}$, $z = X_{Na}^{M4}$ and $f/(y+f) = X_{Fe3+}^{M2}/(X_{Al}^{M2} + X_{Fe3+}^{M2})$. Natural data show a similar partitioning of y and f between actinolite and glaucophane at low f, while there is significant scatter in the data at higher f. Modelling reproduces this partitioning at low f and extrapolates it to $f = 1$.

Fig. 8. Comparison of (a) observed and (b) calculated coexisting actinolite and glaucophane in NCFMASHO at 500 °C. Data are represented in terms of variations in $z = X_{Na}^{M4}$ and $f = X_{Fe3+}^{M2}$. Natural data are restricted to relatively low f, and modelling reproduces the orientation of tie-lines at low f but also extrapolates to $f = 1$.

Thermodynamic properties in NCFMASHO

The adjustments to the end-member properties of the clinoamphiboles were taken to be the same as those in Dale *et al.* (2005) for tremolite, tschermakite and

pargasite (tr = 0, ts = 10 and parg = 15 kJ mol^{-1}). The end-member properties of glaucophane were re-evaluated because of the correlation between glaucophane and magnesioriebeckite that was not considered by Dale *et al.* (2005) . This was done by matching the calculated Fe^{3+}–Al partitioning between coexisting glaucophane, jadeite, epidote and hematite to natural data for Fe_2O_3-rich lithologies from the Tauern Win-
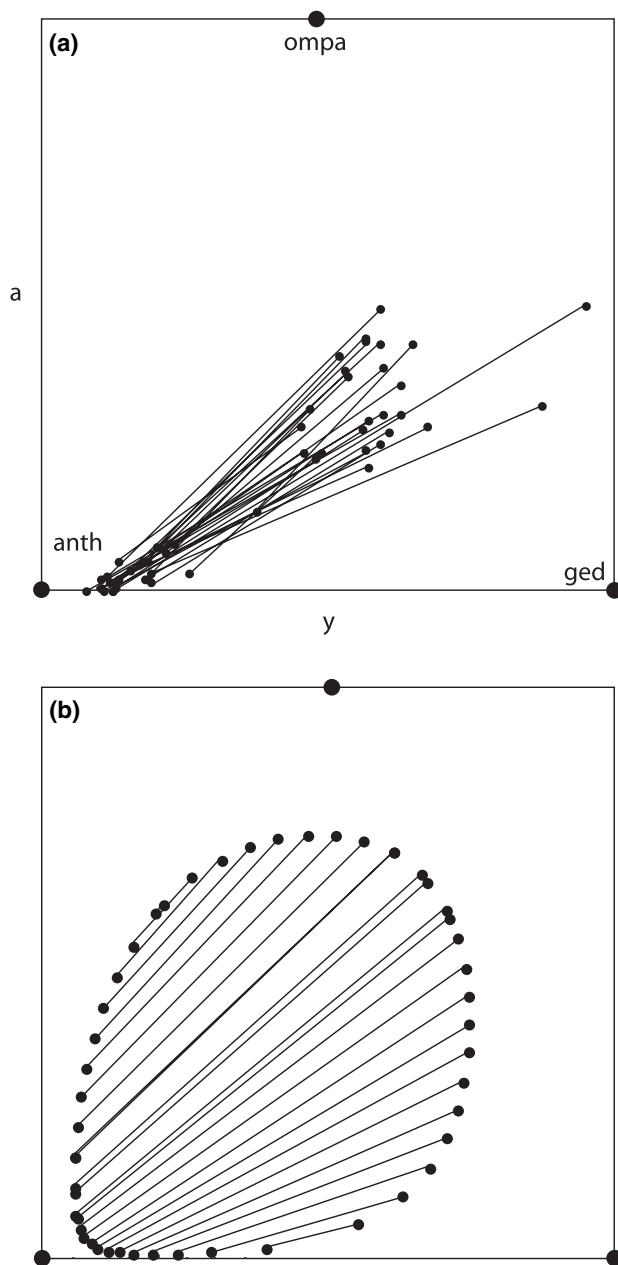
(a)

(b)

Fig. 9. Comparison of (a) observed and (b) calculated coexisting gedrite and anthophyllite at 500 °C. The similarity in the solvus geometry to that of actinolite and hornblende (Dale *et al.*, 2005, fig. 4), suggests that the interaction energies and asymmetry parameters of the orthoamphibole end-members are the same as those of clinoamphibole in NCMASH. Data represented in terms of variations in $y = X_{Al}^{M2}$ and $a = X_{Na}^{A}$.

dow, Austria (Holland & Ray, 1985). The end-member properties were varied until the calculated compositions, Fe^{3+}–Al partitioning and *P–T* conditions matched those reported by Holland & Ray (1985). It was concluded that the $\Delta_f H$ of the glaucophane end-member had to be adjusted by 2–5 kJ mol^{-1} and
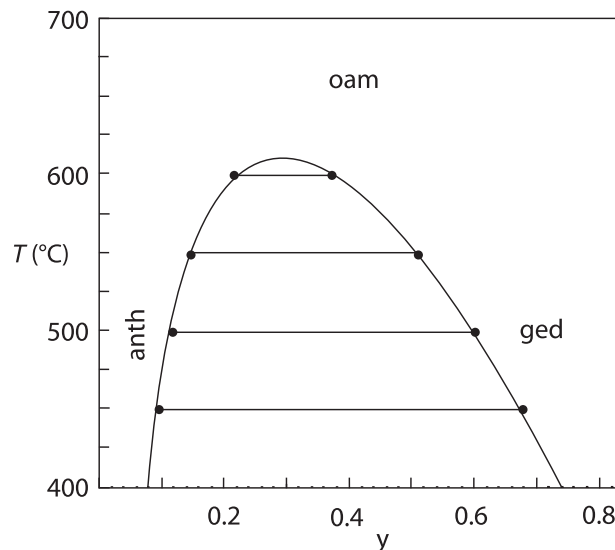
Fig. 10. Calculated coexisting anthophyllite and gedrite showing the size and shape of the orthoamphibole solvus as a function of temperature. The figure illustrates how the solvus narrows with increasing temperature and eventually closes just above 600 °C. Solvus data are plotted in terms of $y = X_{Al}^{M2}$.

magnesioriebeckite by 7–10 kJ mol^{-1} to best fit the natural data.

The ranges for the adjustments to the enthalpies of glaucophane and magnesioriebeckite may appear to be narrow; yet varying the end-member properties only within these ranges leads to dramatic differences in the modelling results. To illustrate this, a pseudosection constructed for a typical MORB composition with the end-member adjustments for glaucophane and magnesioriebeckite taken as 5 and 10 kJ mol^{-1} respectively – rather than the adopted values of 3 and 8 kJ mol^{-1} – is presented in Fig. 14. The bulk composition and all other end-member adjustments used for this calculation are the same as that used in Fig. 18b (see below). With these end-member adjustments, the typical greenschist facies assemblage of actinolite–chlorite–epidote–albite–titanite is stable below 8–10 kbar and 400–480 °C. The high-pressure boundary of this field is defined by the introduction of omphacitic clinopyroxene and also marks the transition from the greenschist to the blueschist facies. However, it is well established from numerous studies that the greenschist–blueschist facies transition in MORB is characterized by the introduction of glaucophane, not omphacite. The dashed line in Fig. 14 is the calculated position of the glaucophane-in boundary and it is clearly metastable with respect to omphacite-bearing assemblages. The result is that, with these values, glaucophane is not present in MORB under blueschist facies conditions. The obvious discrepancy between the modelling and natural data indicates that this particular choice of values is
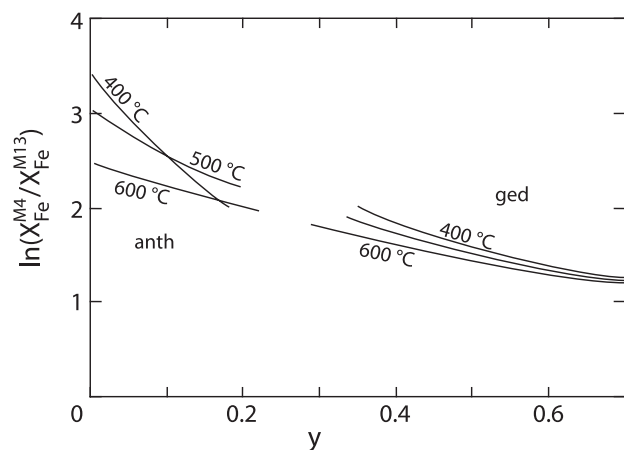
Fig. 11. Calculated partitioning of Fe and Mg between M13 and M4 in orthoamphibole as a function of $y = X_{Al}^{M2}$ and T. Fe–Mg ordering is more pronounced in anthophyllite than gedrite and decreases with increasing y and temperature. The discontinuation in the calculated lines indicates the orthoamphibole solvus.

inappropriate. After further calculations it was concluded that glaucophane should be adjusted by 3 kJ mol^{-1} and magnesioriebeckite by 8 kJ mol^{-1} to reflect the metamorphic facies series in MORB (as shown in Fig. 18b below). This example highlights the sensitivity of pseudosection modelling to the end-member thermodynamics and provides an indication of how well the end-member properties have to be constrained for the model to work.

Apart from anthophyllite, the thermodynamic properties of the orthoamphibole end-members are not well known from experimental data. However, considering that cummingtonite and anthophyllite are polymorphs with near-identical thermodynamic properties, the end-member thermodynamics have to be very precise to be able to correctly predict which of these would be stable for a specific bulk composition. Orthoamphibole end-member properties were initially calibrated using coexisting hornblende–gedrite assemblages. The calibration was then refined until cummingtonite- and anthophyllite-bearing rocks from the literature could be distinguished and the assemblages correctly predicted by pseudosection modelling.

A comparison of the data set of Rabbitt (1948) for wet-chemically analysed orthoamphibole with that of Leake (1968) showed that gedrite has similar ferric iron contents as hornblende. The Al and Na content of coexisting gedrite and hornblende are also of the same order, with gedrite having slightly less Al and Na than hornblende (Robinson *et al.*, 1971, 1982; Spear, 1982). The Ca and X_{Na}^{M4} contents of the orthoamphiboles is very low and therefore the influence of the orthotremolite and orthoglaucophane end-members on the overall stability of orthoamphibole is small. Once the distribution of elements between
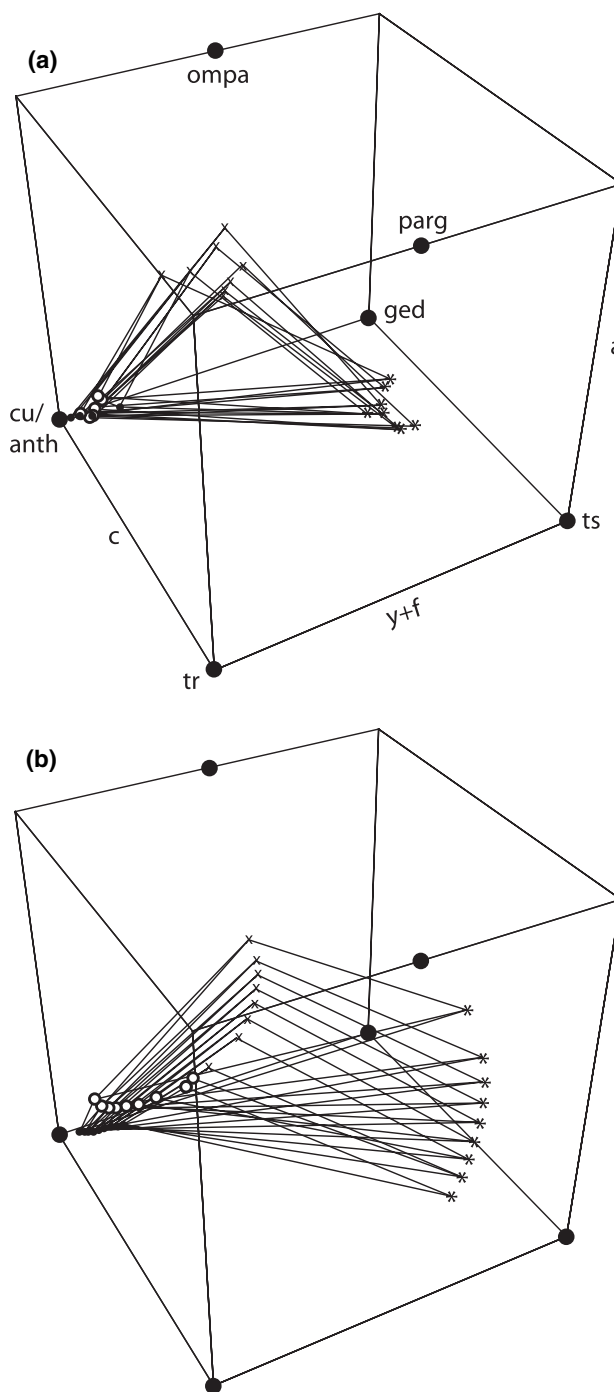

Fig. 12. Comparison of (a) observed and (b) calculated four-amphibole assemblages from Telemark (Stout, 1971, 1972) and the Post Pond Volcanics (Spear, 1980, 1982). Data are represented in terms of variations in $y + f = X_{Al}^{M2} + X_{Fe3+}^{M2}$, $a, = X_{Na}^{A}$ and $c = X_{Ca}^{M4}$ and modelled in NCFMASHO at 500 °C. Hornblende is indicated by stars, gedrite by crosses, anthophyllite by open circles and cummingtonite by filled circles.

gedrite and hornblende matched the natural assemblage data, a series of pseudosections of anthophyllite- and cummingtonite-bearing rocks from the
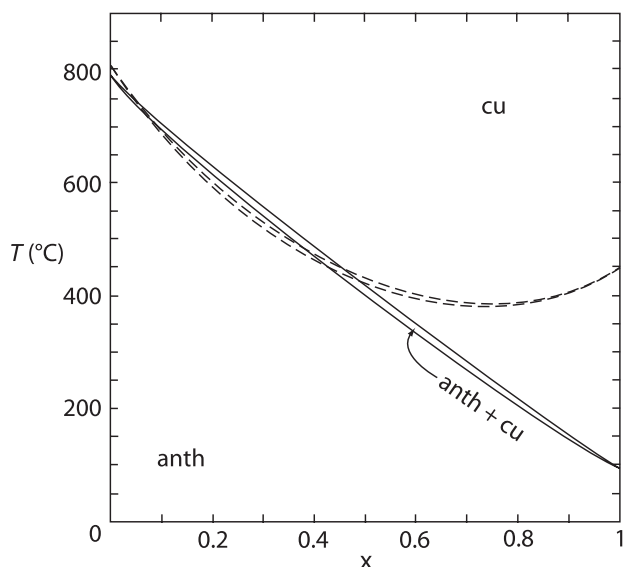
Fig. 13. Calculated transition temperature between cummingtonite and anthophyllite as a function of $x = X_{Fe}^{amph}$ at 5 kbar (solid lines). The cummingtonite–anthophyllite transition of Evans et al. (2001) is shown for comparison (dashed lines).

literature (Miyake, 1984; Schneiderman & Tracy, 1991; Smith et al., 1992; Reche Estrada, 1994) was used in the final calibration of the orthoamphibole end-member thermodynamics (a selection of these is presented and discussed below). It was concluded that the end-member properties required the following adjustments (in kJ mol^{-1}): ged = 23.5, ompa = 28.5, omgl = 15, otr = 0 and omrb = 33. The adjustments to the last four values are with respect to the equivalent clino-derived end-members, and whereas small changes to these values have a more or less dramatic effect on the mineral assemblages in these particular rocks, for the greater majority of rocks the precise values will have little effect.

DISCUSSION

A model for the clino- and orthoamphiboles in a geologically realistic chemical system has been developed primarily using the constraints provided by natural coexisting amphiboles. To illustrate the application of the new models, the results of phase diagram calculations over a range of conditions in the greenschist, epidote-amphibolite, amphibolite and low-pressure blueschist and eclogite facies are presented. These mainly investigate the petrogenetic relationships in 'normal' Ca-rich mafic rocks, with particular emphasis on the differences between the NCFMASH and more realistic NCFMASHTO (T = TiO$_2$) model systems. The petrogenesis of low-Ca amphibolites and associated orthoamphibole- and cummingtonite-bearing rocks will be investigated in

detail in a future contribution and will only be touched on here.

Calculations were performed with THERMOCALC 3.26 (Powell & Holland, 1988, updated July 2006), using the November 2003 updated version of the Holland & Powell (1998) data set (file tcds55.txt). Apart from the amphiboles, phases considered in the modelling and references to the activity models used are diopsidic and omphacitic clinopyroxene (Green et al., 2007), garnet (White et al., 2007), epidote (Holland & Powell, 1998), chlorite (Holland et al., 1998), plagioclase (Holland & Powell, 2003), magnetite (White et al., 2002), ilmenite and hematite (White et al., 2000). Titanite, paragonite, rutile, albite and lawsonite are pure end-member phases.

Petrogenetic grids

The petrogenetic grid for the NCFMASHT system is presented in Fig. 15. TiO$_2$ is considered here because some ilmenite-bearing univariant reactions in NCFMASHTO terminate in this subsystem (see below). The grid is calculated with albite, clinozoisite, titanite, quartz and H$_2$O in excess and the ilmenite-absent part of this grid is equivalent to the NCFMASH grid with albite, clinozoisite, quartz and H$_2$O in excess. The ilmenite-absent part of the NCFMASHT grid has the same topology as the NCFMASH P–T projection calculated by Dale et al. (2005), with all invariant points occurring within 1 kbar and 20 °C of where they were calculated by Dale et al. (2005). A notable difference is that, with the new model, a significant number of reactions occur over a much shorter P–T range and quickly terminate in the NCMASHT or NCFASHT subsystems. This is because the two subsystems now have the same non-ideality, allowing the amphiboles to change x more rapidly with changing temperature.

The addition of ferric iron not only affects the silicate minerals, but also allows for the addition of new phases such as hematite and magnetite. However, to model the FeO–Fe$_2$O$_3$–TiO$_2$ oxide minerals properly, TiO$_2$ has to be considered as well (e.g. White et al., 2000). In the more realistic NCFMASHTO system, the effect of ferric iron on the stability of amphibole, clinopyroxene (diopside and omphacite), epidote and garnet as well as the influence of important accessory phases, such as titanite, rutile, ilmenite, magnetite and hematite, can be quantitatively assessed. The NCFMASHTO petrogenetic grid (Fig. 16) has a similar topology to that of the ferric-free system but is more complex because it also involves different combinations of the oxide phases. Upon the addition of ferric iron to the NCFMASHT P–T projection in Fig. 15, each of the invariant points in this system becomes a univariant reaction that extends into the ferric-bearing system (Fig. 16). These reactions continue until a_{O_2} becomes high enough to stabilize an
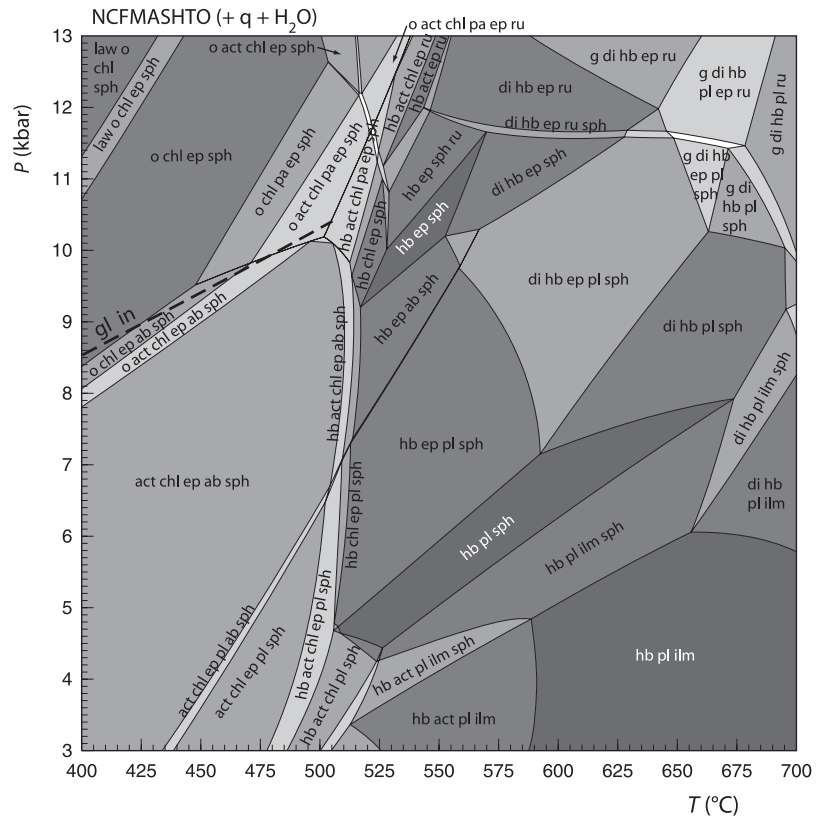
Fig. 14. Calculated *P–T* pseudosection for the same MORB composition as in Fig. 18b, but with the end-member adjustments to glaucophane and magnesioriebeckite taken as 5 and 10 kJ mol⁻¹ respectively. With these values, the glaucophane phase boundary (dashed line) is metastable with respect to omphacitic clinopyroxene and glaucophane is not present under blueschist facies conditions. These end-member adjustments are inappropriate because natural data indicate that glaucophane, not omphacite, should be present at these conditions.
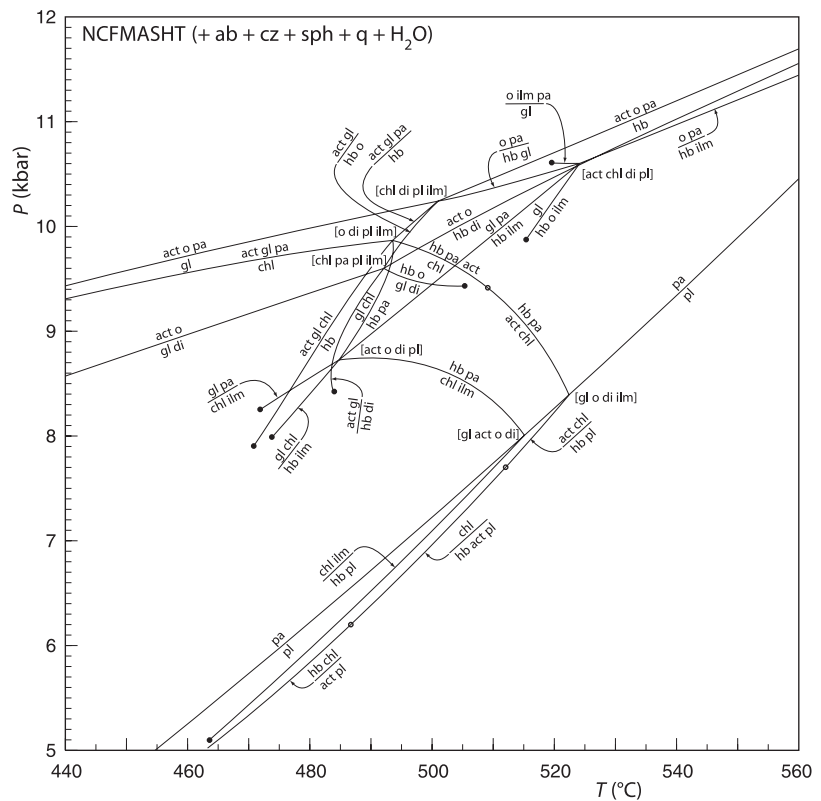
Fig. 15. Calculated petrogenetic grid for the NCFMASHT system with albite, clinozoisite, titanite, quartz and H₂O in excess. Singularities are indicated by open circles and the point where reactions terminate in the NCFASHT subsystem are indicated by solid circles.
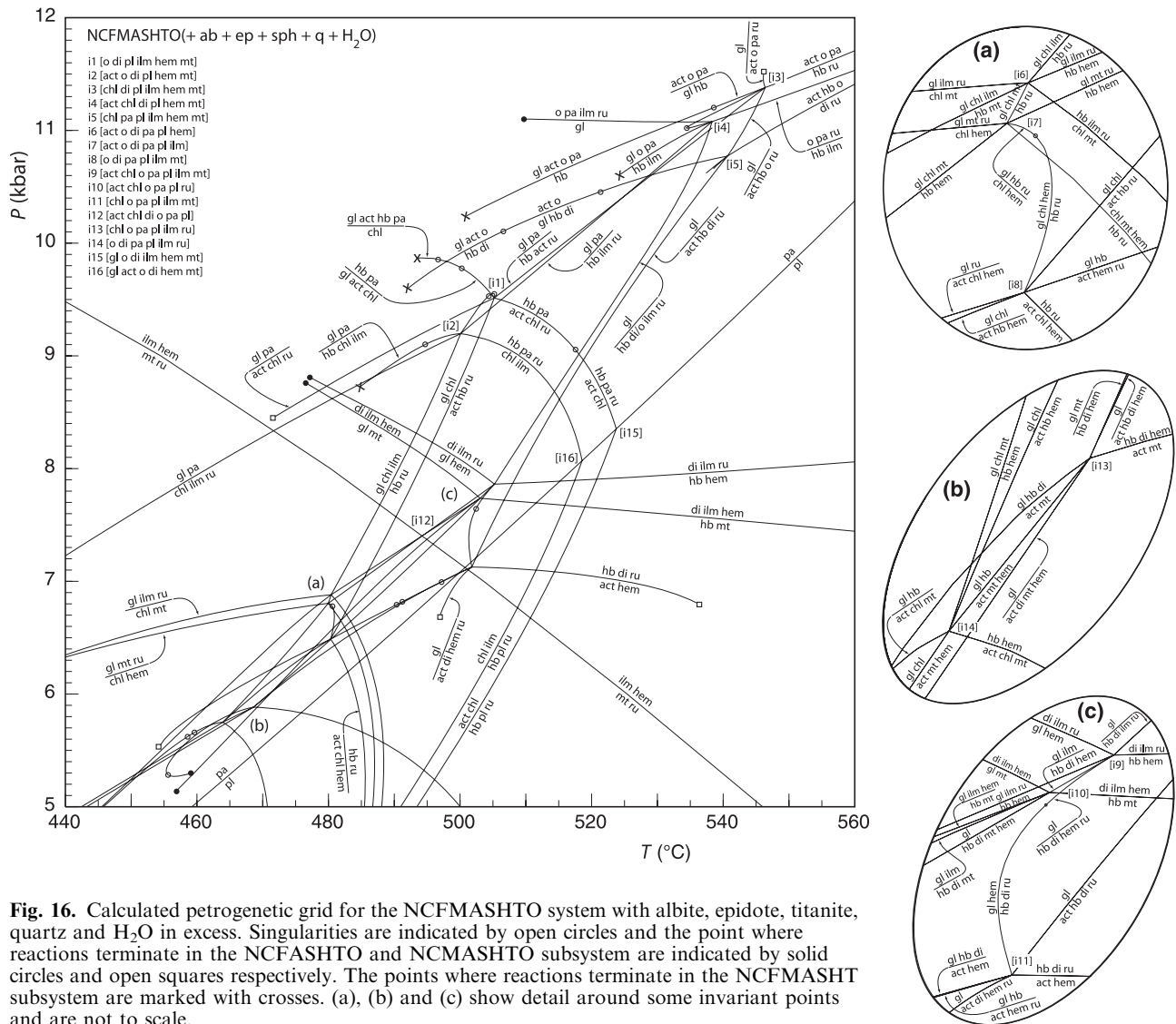
Fig. 16. Calculated petrogenetic grid for the NCFMASHTO system with albite, epidote, titanite, quartz and H_2O in excess. Singularities are indicated by open circles and the point where reactions terminate in the NCFASHTO and NCMASHTO subsystem are indicated by solid circles and open squares respectively. The points where reactions terminate in the NCFMASHT subsystem are marked with crosses. (a), (b) and (c) show detail around some invariant points and are not to scale.

additional oxide phase (rutile) and form new NCFMASHTO invariant points.

To illustrate the expansion from NCFMASHT to NCFMASHTO, consider the NCFMASHT invariant point involving glaucophane, actinolite, hornblende, chlorite and paragonite that occurs at 9.9 kbar and 495 °C (labelled [o di pl ilm] in Fig. 15). Upon the addition of ferric iron, a univariant reaction extends from this ferric-free invariant to a rutile-bearing invariant point in NCFMASHTO at 9.5 kbar and 505 °C (labelled as [i1] in Fig. 16). From this rutile-bearing invariant, along the actinolite-absent univariant, an ilmenite-bearing invariant point is stabilized at 9.2 kbar and 500 °C (labelled as [i2] in Fig. 16). Similarly, a hematite-bearing invariant point is encountered along the paragonite-absent univariant at 6.4 kbar and 480 °C (labelled as [i8] in Fig. 16).

Because the addition of ferric iron increases the stability of glaucophane relative to that of the other amphiboles, the Fe_2O_3-rich hematite-bearing invariant point occurs at significantly lower pressure and temperature than in the ferric-free system (Figs 15 & 16). However, it does not imply that the Fe_2O_3-rich low-pressure reactions will ever be encountered by normal rock compositions that have relatively low Fe_2O_3 contents.

To provide some indication of which parts of the NCFMASHTO grid might be applicable to crustal rocks, the quartz–fayalite–magnetite (QFM) and hematite–magnetite (HM) buffers are overlaid on the grid (Fig. 17). These buffers, widely used in experimental petrology, are considered to bracket a_{O_2} for most crustal rocks (e.g. Spear, 1993). Most of the univariant reactions that emanate from the ferric-free
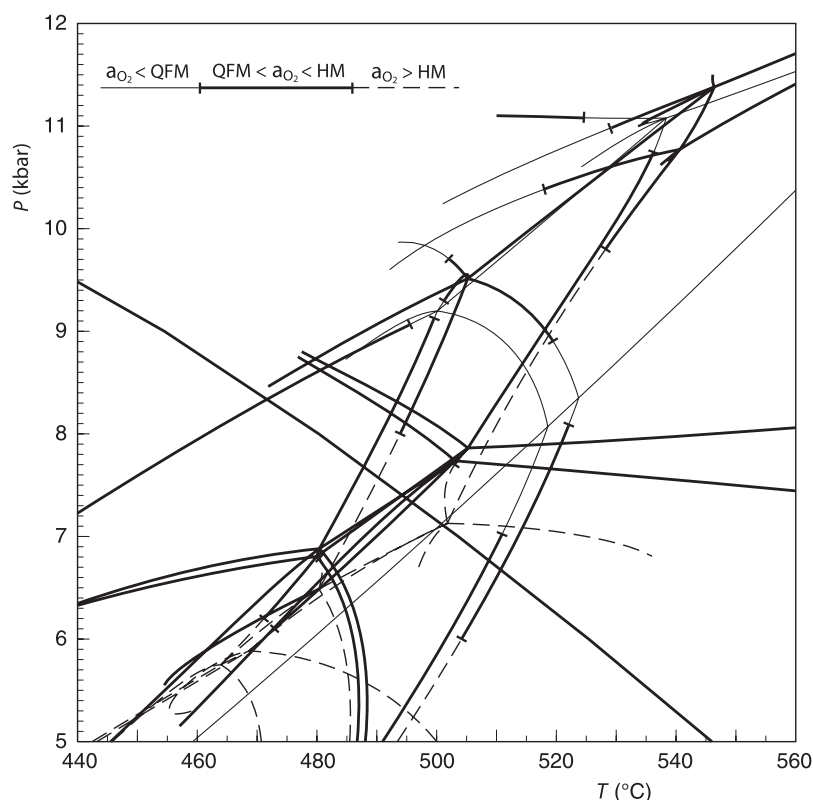
Fig. 17. The QFM and HM buffers overlaid on the NCFMASHTO petrogenetic grid, showing which parts of the grid have a_{O_2} lower than the QFM buffer (thin solid lines), for which parts of the grid a_{O_2} is between QFM and HM (thick solid lines) and for which parts a_{O_2} is higher than HM (thin dashed lines).

system intersect the QFM buffer before they reach an NCFMASHTO invariant point (Fig. 17). However, four of the NCFMASHTO invariants occur at a_{O_2} below that of the QFM buffer (labelled as [i2], [i4], [i15] and [i16] in Fig. 16). Similarly, four invariant points occur at a_{O_2} above that of the HM buffer (labelled as [i8], [i11], [i13] and [i14] in Fig. 16). The remaining NCFMASHTO invariants are within the range of a_{O_2} that could be expected in crustal rocks and might therefore be observed in natural assemblages.
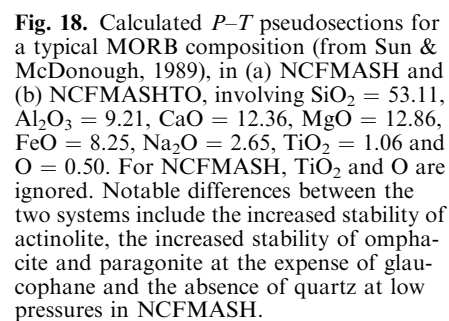
Pseudosections

Pseudosections show the multivariant phase relationships for a chosen rock composition as a function of P–T. A series of pseudosections based on a typical MORB composition (sample 104-16 of Sun & McDonough, 1989) were constructed to further illustrate the differences between the NCFMASH and NCFMASHTO systems (Fig. 18). For calculations in NCFMASH, K_2O, MnO and TiO_2 in the rock composition were ignored and all Fe was assumed to be FeO. For calculations in NCFMASH-TO, the small amounts of K_2O and MnO were ignored. The analysis was then recalculated assuming that 12% of the total Fe was present as Fe_2O_3, a value typical for wet-chemical analyses of MORB (e.g. Schilling et al., 1983) that also corresponds to

an a_{O_2} slightly higher than the QFM buffer in our calculations.

Whereas there is a good overall agreement between the pseudosections in the two systems, there are also marked differences (Fig. 18). In NCFMASH, because of the absence of ferric iron, the stability of glaucophane is significantly reduced to the benefit of omphacite and paragonite relative to the ferric-bearing system. The stability field of actinolite is greater in NCFMASH than in NCFMASHTO, to the point that actinolite is predicted to coexist with diopsidic clinopyroxene in a narrow field between 525 and 575 °C and 6–10 kbar (Fig. 18a). This is partly because Ti is not considered and the Ca that would have been sequestered by titanite is available to stabilize actinolite. Finally, because of the absence of oxide phases in NCFMASH, the ratio of Si to the ferromagnesian elements is reduced compared with the bigger system. This results in large areas of the NCFMASH pseudosection being quartz absent, particularly at low pressures (Fig. 18a).

The effect of ferric iron on the pressure of the greenschist–blueschist facies transition can be seen in a P–$X_{Fe^{3+}}$ section based on the MORB composition and constructed for variable Fe_2O_3 at a fixed temperature of 450 °C (Fig. 19). Note that the compositional variable in Fig. 19 is the amount of Fe_2O_3, not a_{O_2}, and that the bulk rock Fe^{2+}/Mg ratio is constant. The glaucophane-in boundary occurs at 9.4 kbar in the
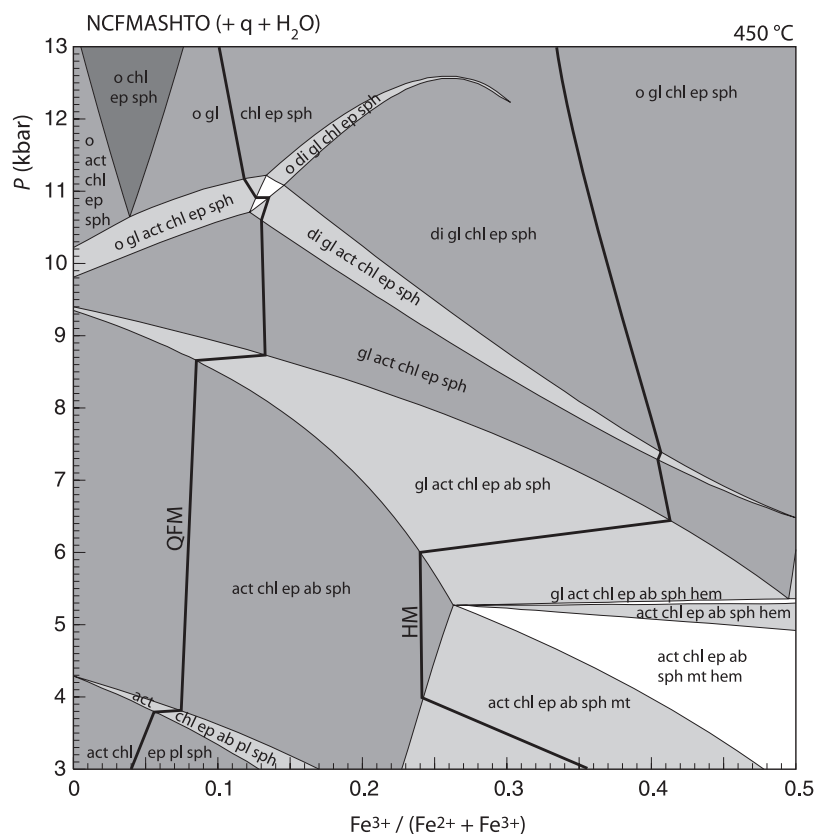
(a)

NCFMASH (+ q + H₂O)

(b)

NCFMASHTO (+ q + H₂O)

Fig. 18. Calculated *P–T* pseudosections for a typical MORB composition (from Sun & McDonough, 1989), in (a) NCFMASH and (b) NCFMASHTO, involving SiO_2 = 53.11, Al_2O_3 = 9.21, CaO = 12.36, MgO = 12.86, FeO = 8.25, Na_2O = 2.65, TiO_2 = 1.06 and O = 0.50. For NCFMASH, TiO_2 and O are ignored. Notable differences between the two systems include the increased stability of actinolite, the increased stability of omphacite and paragonite at the expense of glaucophane and the absence of quartz at low pressures in NCFMASH.

Fig. 19. Calculated $P-X_{Fe^{3+}}$ pseudosection based on a typical MORB composition (from Sun & McDonough, 1989) with variable Fe_2O_3 at 450 °C. With increasing Fe_2O_3, the greenschist–blueschist facies transition is displaced down pressure from 9.4 to 5.3 kbar, before it is buffered by hematite at $X_{Fe^{3+}} = 0.25$. Increasing Fe_2O_3 also stabilizes diopside at the expense of omphacite at $X_{Fe^{3+}} = 0.13$. The pseudosection in Fig. 18b is drawn at $X_{Fe^{3+}} = 0.12$ and the positions of the QFM and HM buffers are shown for reference. The bulk composition varies along the x-axis from $SiO_2 = 53.92$, $Al_2O_3 = 9.35$, $CaO = 12.55$, $MgO = 13.06$, $FeO = 7.36$, $Na_2O = 2.69$, $TiO_2 = 1.08$ and $O = 0$ to $SiO_2 = 48.56$, $Al_2O_3 = 8.42$, $CaO = 11.30$, $MgO = 11.76$, $FeO = 13.26$, $Na_2O = 2.42$, $TiO_2 = 0.97$ and $O = 3.31$.

ferric-free system, and moves down P upon the addition of Fe_2O_3. Once the bulk composition is ferric enough for the greenschist facies assemblage to be buffered by hematite and magnetite, the glaucophane phase boundary has decreased by more than 4 kbar so that the greenschist–blueschist transition occurs at 5.3 kbar.

The phase relationships for cummingtonite- and orthoamphibole-bearing amphibolites are illustrated with examples from the Uvete area in central Kenya that were investigated by Miyake (1984). These rocks were chosen because they exhibit a range of assemblages varying from Ca-rich garnet–diopside–hornblende amphibolites to low-Ca garnet–cummingtonite–hornblende and garnet–gedrite–anthophyllite–hornblende rocks that were equilibrated at the same $P-T$ conditions (Miyake, 1984). Pseudosection modelling of the two low-Ca rock types (Fig. 20) reveals that the observed peak metamorphic assemblages occur over small stability fields at conditions around 9 kbar and 650 °C in both samples. Including Mn in the model system is likely to move the stability field of garnet down $P-T$, which would increase the $P-T$ range over which these peak assemblages occur.

In the lower amphibolite facies, both rock types consist of hornblende–chlorite–plagioclase–ilmenite assemblages. With increasing temperature, depending on the bulk composition, either anthophyllite or cummingtonite will be stabilized. In the cummingtonite-bearing sample (Fig. 20a), cummingtonite is the only low-Ca amphibole and it persists to the peak $P-T$ conditions at $\sim$9 kbar and 650 °C. However, in the orthoamphibole-bearing sample the composition of the orthoamphibole changes from anthophyllite to gedrite at the point where chlorite breaks down (around 625 °C; Fig. 20b). At this temperature, there is complete solid solution between anthophyllite and gedrite and the transition does not involve the crossing of a solvus. The transition extends up pressure with increasing temperature, as shown by the dashed line in Fig. 20b. Miyake (1984) reported that this sample contains both anthophyllite and gedrite, with anthophyllite occurring as inclusions in gedrite. From the pseudosection modelling, it would appear that anthophyllite and gedrite are unlikely to constitute an equilibrium assemblage, but rather represent a preserved prograde texture.

CONCLUSIONS

With the development of realistic models for the amphiboles and other mafic phases such as clinopyroxene (Green *et al.*, 2007), it is now possible to model mafic rocks in geologically appropriate systems such as NCFMASHTO. This allows, for the first time, the petrology of mafic rocks to be investigated with the same kind of veracity as has been possible for pelitic

(a) NCFMASHTO (+ q + H₂O)

(b) NCFMASHTO (+ q + H₂O)

Fig. 20. Calculated *P–T* pseudosections for (a) cummingtonite-bearing and (b) ortho-amphibole-bearing low-Ca amphibolites from central Kenya (Miyake, 1984). The composition of (a) is $SiO_2 = 68.07$, $Al_2O_3 = 8.49$, $CaO = 4.71$, $MgO = 4.97$, $FeO = 7.49$, $Na_2O = 4.71$, $TiO_2 = 1.12$ and $O = 0.44$; and for (b) is $SiO_2 = 65.14$, $Al_2O_3 = 8.79$, $CaO = 4.49$, $MgO = 9.22$, $FeO = 6.94$, $Na_2O = 4.23$, $TiO_2 = 0.79$ and $O = 0.39$.

systems (e.g. White *et al.*, 2003, 2004, 2005). As with the metapelites (White *et al.*, 2007), it makes petrological sense to do calculations in the largest chemical system available, as was illustrated above for the MORB composition (Fig. 18), where significant differences in the results were obtained by ignoring apparently minor components such as TiO_2 and Fe_2O_3.

ACKNOWLEDGEMENTS

REFERENCES

Baldwin, J. A., Powell, R., Williams, M. L. & Goncalves, P., 2007. Formation of eclogite, and reaction during exhumation to mid-crustal levels, Snowbird tectonic zone, western Canadian Shield. *Journal of Metamorphic Geology*, in press.

Brady, J., 1974. Coexisting actinolite and hornblende from west-central New Hampshire. *American Mineralogist*, **59**, 529–535.

Cameron, K. L., 1975. An experimental study of actinolite–cummingtonite phase relations with notes on the synthesis of Fe-anthophyllite. *American Mineralogist*, **60**, 375–390.

Carson, C. J. & Powell, R., 1997. Garnet-orthopyroxene geothermometry and geobarometry: error propagation and equilibration effects. *Journal of Metamorphic Geology*, **15,** 679–686.

Carson, C. J., Powell, R. & Clarke, G. L., 1999. Calculated mineral equilibria for eclogites in CaO–Na$_2$O–FeO–MgO–Al$_2$O$_3$–SiO$_2$–H$_2$O: application to the Pouébo Terrane, Pam Peninsula, New Caledonia. *Journal of Metamorphic Geology*, **17**, 9–24.

Clark, M. D., 1978. Amphibolitic rocks from the Precambrian of Grand Canyon: mineral chemistry and phase petrology. *Mineralogical Magazine*, **42**, 199–207.

Clarke, G. L., Powell, R. & Fitzherbert, J. A., 2006. The lawsonite paradox: a comparison of field evidence and mineral equilibria modelling. *Journal of Metamorphic Geology*, **24**, 715–725.

Dale, J., Powell, R., White, R. W., Elmer, F. L. & Holland, T. J. B., 2005. A thermodynamic model for Ca–Na clinoamphiboles in Na$_2$O–CaO–FeO–MgO–Al$_2$O$_3$–SiO$_2$–H$_2$O–O for petrological calulations. *Journal of Metamorphic Geology*, **23**, 771–791.

Driscall, J., Jenkins, D. M., Dyar, M. D. & Bozhilov, K. N., 2005. Cation ordering in synthetic low-calcium actinolite. *American Mineralogist*, **90**, 900–911.

Dymek, R. F. & Klein, C., 1988. Chemistry, petrology and origin of banded iron-formation lithologies from the 3800 Ma Isua supracrustal belt, West Greenland. *Precambrian Research*, **39**, 247–302.

Elmer, F. L., White, R. W. & Powell, R., 2006. Devolatilisation of metabasic rocks during greenschist-amphibolite facies metamorphism. *Journal of Metamorphic Geology*, **24**, 497–513.

Evans, B. W. & Ghiorso, M. S., 1995. Thermodynamics and petrology of cummingtonite. *American Mineralogist*, **80**, 649–663.

Evans, B. W. & Yang, H., 1998. Fe–Mg order–disorder in tremolite–actinolite–ferro-actinolite at ambient and high temperature. *American Mineralogist*, **83**, 458–475.

Evans, B. W., Ghiorso, M. S., Yang, H. & Medenbach, O., 2001. Thermodynamics of the amphiboles; anthophyllite–ferro-anthophyllite and the ortho–clino phase loop. *American Mineralogist*, **86**, 640–651.

Frimmel, H. E., 1996. Witwatersrand iron-formations and their significance for gold genesis and the composition limits of orthoamphibole. *Mineralogy and Petrology*, **56**, 273–295.

Ghiorso, M. S. & Evans, B. W., 2002. Thermodynamics of the amphiboles; Ca–Mg–Fe^{2+} quadrilateral. *American Mineralogist*, **87**, 79–98.

Gole, M. J. & Klein, C., 1981. High-grade metamorphic Archaean banded iron-formations, Western Australia: assemblages with coexisting pyroxenes ± fayalite. *American Mineralogist*, **66**, 87–99.

Green, E. C. R., Holland, T. J. B. & Powell, R., 2007. An order–disorder model for omphacitic pyroxenes in the system jadeite–diopside–hedenbergite–acmite, with applications to eclogitic rocks. *American Mineralogist*, in press.

Hawthorne, F. C., Griep, J. L. & Curtis, L., 1980. A three-amphibole assemblage from the Tallan Lake Sill, Peterborough County, Ontario. *Canadian Mineralogist*, **18**, 275–284.

Hirschmann, M., Evans, B. W. & Yang, H., 1994. Composition and temperature dependence of Fe–Mg ordering in cummingtonite–grunerite as determined by X-ray diffraction. *American Mineralogist*, **79**, 862–877.

Holdaway, M. J., 1972. Thermal stability of Al–Fe epidote as a function of fo_2 and Fe content. *Contributions to Mineralogy and Petrology*, **37**, 307–340.

Holland, T. J. B. & Blundy, J., 1994. Non-ideal interactions in calcic amphiboles and their bearing on amphibole–plagioclase thermometry. *Contributions to Mineralogy and Petrology*, **116**, 433–447.

Holland, T. J. B. & Powell, R., 1996a. Thermodynamics of order-disorder in minerals. I. Symmetric formalism applied to minerals of fixed composition. *American Mineralogist*, **81**, 1413–1424.

Holland, T. J. B. & Powell, R., 1996b. Thermodynamics of order–disorder in minerals. II. Symmetric formalism applied to solid solutions. *American Mineralogist*, **81**, 1425–1437.

Holland, T. J. B. & Powell, R., 1998. An internally consistent thermodynamic dataset for phases of petrological interest. *Journal of Metamorphic Geology*, **16**, 309–343.

Holland, T. J. B. & Powell, R., 2003. Activity–composition relations for phases in petrological calculations: an asymmetric multicomponent formulation. *Contributions to Mineralogy and Petrology*, **145**, 492–501.

Holland, T. J. B. & Powell, R., 2006. Mineral activity–composition relations and petrological calculations involving cation equipartition in multisite minerals: a logical inconsistency. *Journal of Metamorphic Geology*, **24**, 851–861.

Holland, T. J. B. & Ray, N. J., 1985. Glaucophane and pyroxene breakdown reactions in the Pennine units of the Eastern Alps. *Journal of Metamorphic Geology*, **3**, 417–438.

Holland, T. J. B., Baker, J. M. & Powell, R., 1998. Mixing properties and activity–composition relationships of chlorites in the system MgO–FeO–Al$_2$O$_3$–SiO$_2$–H$_2$O. *European Journal of Mineralogy*, **10**, 395–406.

Hollocher, K., 1991. Prograde amphibole dehydration reactions during high-grade regional metamorphism, central Massachusetts, U.S.A. *American Mineralogist*, **76**, 956–970.

Immega, I. P. & Klein, C., 1976. Mineralogy and petrology of some Precambrian iron-formations in southwestern Montana. *American Mineralogist*, **61**, 1117–1144.

James, R. S., Grieve, R. A. F. & Pauk, L., 1978. The petrology of cordierite–anthophyllite gneisses and associated mafic and pelitic gneisses at Manitouwadge, Ontario. *American Journal of Science*, **278**, 41–63.

Jenkins, D. M. & Bozhilov, K. N., 2003. Stability and thermo-dynamic properties of ferro-actinolite: a re-investigation. *American Journal of Science*, **303,** 723–752.

Kahl, W.-A. & Schumacher, J. C., 2000. Multiple pyroxene and amphibole assemblages in the amphibolite facies; bulk compositional controls. *American Mineralogist*, **85,** 1606–1616.

Leake, B. E., 1968. *A catalog of analyzed calciferous and sub-calciferous amphiboles together with their nomenclature and associated minerals.* Special Paper 68, Geological Society of America, 210 pp.

Liu, J. & Bohlen, S. R., 1995. Mixing properties and stability of jadeite–acmite pyroxene in the presence of albite and quartz. *Contributions to Mineralogy and Petrology*, **119,** 433–440.

Mitchell, J. T., Bloss, F. D. & Gibbs, G. V., 1970. A refinement of the structure of actinolite. *American Mineralogist*, **55,** 302–303.

Miyake, A., 1984. Phase equilibria in the hornblende-bearing basic gneisses of the Uvete area, central Kenya. *Journal of Metamorphic Geology*, **2,** 165–177.

Oba, T. & Nicholls, I. A., 1986. Experimental study of cum-mingtonite and Ca–Na amphibole relations in the system Cum–Act–Pl–Qz–H_2O. *American Mineralogist*, **71,** 1354–1365.

Papike, J. J. & Ross, M., 1970. Gedrites: crystal structures and intracrystalline cation distributions. *American Mineralogist*, **55,** 1945–1972.

Popp, R. K. & Gilbert, M. C., 1972. Stability of acmite–jadeite pyroxenes at low pressures. *American Mineralogist*, **57,** 1210–1231.

Powell, R., 1977. Activity–composition relationships for crys-talline solutions. In: *Thermodynamics in Geology* (ed. Fraser, D.), pp. 57–65. D. Riedel, London.

Powell, R. & Holland, T. J. B., 1988. An internally consistent thermodynamic dataset with uncertainties and correlations: 3. Application, methods, worked examples and a computer program. *Journal of Metamorphic Geology*, **6,** 173–204.

Powell, R. & Holland, T. J. B., 1993. On the formulation of simple mixing models for complex phases. *American Miner-alogist*, **78,** 1174–1180.

Powell, R. & Holland, T. J. B., 1999. Relating formulations of the thermodynamics of mineral solid solutions: activity modeling of pyroxenes, amphiboles and micas. *American Mineralogist*, **84,** 1–14.

Rabbitt, J. C., 1948. A new study of the anthophyllite series. *American Mineralogist*, **33,** 263–323.

Reche Estrada, J., 1994. El metamorfismo de medio-alto grado de las anfibolitas COR: aporte de nuevos datos naturales, recopilación de datos empíricos y construcción de un nuevo modelo petrogenético. PhD thesis, Universitat Autònoma de Barcelona.

Robinson, P. & Jaffe, H. W., 1969. Aluminous enclaves in gedrite-cordierite gneiss from southwestern New Hampshire. *American Journal of Science*, **267,** 389–421.

Robinson, P., Jaffe, H. W., Klein, C. & Ross, M., 1969. Equi-librium coexistence of three amphiboles. *Contributions to Mineralogy and Petrology*, **22,** 248–258.

Robinson, P., Ross, M. & Jaffe, H. W., 1971. Composition of the anthophyllite-gedrite series, comparisons of gedrite and hornblende, and the anthophyllite–gedrite solvus. *American Mineralogist*, **56,** 1005–1041.

Robinson, P., Spear, F. S., Schumacher, J. C. *et al.*, 1982. Phase relations of metamorphic amphiboles: natural occurrence and theory. In: *Reviews in Mineralogy* (eds Veblin, D. & Ribbe, P.), Vol. 9B, pp. 1–211. Mineralogical Society of America, Washington, DC.

Sampson, G. A. & Fawcett, J. J., 1977. Coexisting amphiboles from the Hastings region of southwestern Ontario. *Canadian Mineralogist*, **15,** 283–296.

Schilling, J.-G., Zajec, M., Evans, R. *et al.*, 1983. Petrologic and geochemical variations along the Mid-Atlantic Ridge from 27 °N to 73 °N. *American Journal of Science*, **283,** 510–586.

Schneiderman, J. S. & Tracy, R. J., 1991. Petrology of ortho-amphibole–cordierite gneisses from the Orijärvi area, South-west Finland. *American Mineralogist*, **76,** 942–955.

Seifert, F., 1978. Equilibrium Mg–Fe^{2+} cation distribution in anthophyllite. *American Journal of Science*, **278,** 1323–1333.

Seifert, F. & Virgo, D., 1975. Kinetics of the Fe^{2+}–Mg order–disorder reaction in anthophyllites: quantitative cooling rates. *Science*, **188,** 1107–1109.

Smith, M. S., Dymek, R. F. & Schneiderman, J. S., 1992. Implications of trace element geochemistry for the origin of cordierite–anthophyllite rocks from Orijärvi, SW Finland. *Journal of Geology*, **100,** 545–559.

Spear, F. S., 1980. The gedrite–anthophyllite solvus and the composition limits of orthoamphibole from the Post Pond Volcanics, Vermont. *American Mineralogist*, **65,** 1103–1118.

Spear, F. S., 1982. Phase equilibria of amphibolites from the Post Pond Volcanics, Mt. Cube Quadrangle, Vermont. *Jour-nal of Petrology*, **23,** 383–426.

Spear, F. S., 1993. *Metamorphic Phase Equilibria and Pressure–Temperature–Time Paths*, Mineralogical Society of America, Washington, DC, 799 pp.

Srikantappa, C., Raith, M. & Ackermand, D., 1985. High-grade regional metamorphism of ultramafic and mafic rocks from the Archaean Sargur terrane, Karnataka, South India. *Pre-cambrian Research*, **30,** 189–219.

Štípská, P. & Powell, R., 2005. Constraining the *P–T* path of a MORB-type eclogite using pseudosections, garnet zoning and garnet-clinopyroxene thermometry: an example from the Bohemian Massif. *Journal of Metamorphic Geology*, **23,** 725–743.

Štípská, P., Pitra, P. & Powell, R., 2006. Separate or shared metamorphic histories of eclogite and surrounding rocks? An example from the Bohemian Massif. *Journal of Metamorphic Geology*, **24,** 219–240.

Stephenson, N. C. N. & Hensel, H. D., 1979. Intergrown calcic and Fe–Mg amphiboles from the Wongwibinda metamorphic complex, N.S.W., Australia. *Canadian Mineralogist*, **17,** 11–23.

Stout, J. H., 1971. Four coexisting amphiboles from Telemark, Norway. *American Mineralogist*, **56,** 212–224.

Stout, J. H., 1972. Phase petrology and mineral chemistry of coexisting amphiboles from Telemark, Norway. *Journal of Petrology*, **13,** 99–145.

Sun, S.-S. & McDonough, W. F., 1989. Chemical and isotopic systematics of oceanic basalts: implications for mantle com-positions and processes. In: *Magmatism in the Ocean Basins*, Special Publications (eds Saunders, A. & Norry, M.), Vol. 42, pp. 313–345. Geological Society, London.

Wei, C. J., Powell, R. & Zhang, L. F., 2003. Calculated mineral equilibria for eclogites from the south Tianshan, NW China. *Journal of Metamorphic Geology*, **21,** 163–180.

White, R. W., Powell, R., Holland, T. J. B. & Worley, B. A., 2000. The effect of TiO_2 and Fe_2O_3 on metapelitic assemblages at greenschist and amphibolite facies conditions: mineral equilibria calculations in the system K_2O–FeO–MgO–Al_2O_3–SiO_2–H_2O–TiO_2–Fe_2O_3. *Journal of Metamorphic Geology*, **18,** 497–511.

White, R. W., Powell, R. & Clarke, G. L., 2002. The interpret-ation of reaction textures in Fe-rich metapelitic granulites of the Musgrave Block, central Australia: constraints from mineral equilibria calculations in the system K_2O–FeO–MgO–Al_2O_3–SiO_2–H_2O–TiO_2–Fe_2O_3. *Journal of Metamorphic Geology*, **20,** 41–55.

White, R. W., Powell, R. & Clarke, G. L., 2003. Prograde meta-morphic assemblage evolution during partial melting of meta-sedimentary rocks at low pressures: migmatites from Mt Stafford, central Australia. *Journal of Petrology*, **44,** 1937–1960.

White, R. W., Powell, R. & Halpin, J. A., 2004. Spatially-fo-cused melt formation in aluminous metapelites from Broken Hill, Australia. *Journal of Metamorphic Geology*, **22,** 825–845.

White, R. W., Pomroy, N. E. & Powell, R., 2005. An *in situ* metatexite–diatexite transition in upper amphibolite facies

rocks from Broken Hill, Australia. *Journal of Metamorphic Geology*, **23**, 579–602.

White, R. W., Powell, R. & Holland, T. J. B., 2007. Progress relating to calculation of partial melting equilibria for metapelites and felsic gneisses. *Journal of Metamorphic Geology*, **25**, 511–527.

Wiser, N. M. & Wood, B. J., 1991. Experimental determination of activities in Fe–Mg olivine at 1400 K. *Contributions to Mineralogy and Petrology*, **108**, 146–153.

Yang, J.-J. & Powell, R., 2006. Calculated phase relations in the system Na$_2$O–CaO–K$_2$O–FeO–MgO–Al$_2$O$_3$–SiO$_2$–H$_2$O with applications to UHP eclogites and whiteschists. *Journal of Petrology*, **47**, 2047–2071.

APPENDIX 1: DEPENDENT END-MEMBERS IN THE ASYMMETRIC FORMALISM

An unfortunate error of logic occurs in Dale *et al.* (2005) regarding the thermodynamics of mixing involving dependent sets of end-members in the asymmetric formalism. The following expressions correct that error. In the asymmetric formalism, the non-configurational energy (G^*) can be written

$$G^* = \sum_{i=1}^{n-1} p_i G_i + \left(\sum_{\ell=1}^{n} \alpha_\ell p_\ell \right) \left(\sum_{i=1}^{n-1} \sum_{j=i+1}^{n} \phi_i \phi_j \frac{2w_{ij}}{\alpha_i + \alpha_j} \right) \quad (7)$$

in which G_i is the Gibbs energy of end-member i, p_i is the proportion of end-member i, ϕ_i is effectively a size-parameter-adjusted proportion

$$\phi_i = \frac{\alpha_i p_i}{\sum_{k=1}^{n} \alpha_k p_k}$$

and n being the number of end-members in the independent set. Writing the Gibbs energies of the end-members as a vector, g, the van Laar size parameters as a vector, α, and a strictly upper triangular matrix, W, defined by:

$$W = \begin{pmatrix} 0 & \frac{2w_{12}}{\alpha_1+\alpha_2} & \frac{2w_{13}}{\alpha_1+\alpha_3} & \cdots & \frac{2w_{1n}}{\alpha_1+\alpha_n} \\ 0 & 0 & \frac{2w_{23}}{\alpha_2+\alpha_3} & \cdots & \frac{2w_{2n}}{\alpha_2+\alpha_n} \\ 0 & 0 & 0 & \cdots & \frac{2w_{3n}}{\alpha_3+\alpha_n} \\ \vdots & \vdots & \vdots & \ddots & \vdots \\ 0 & 0 & 0 & \cdots & 0 \end{pmatrix} \quad (8)$$

then Eq. (7) can be written as the matrix equation

$$G^* = p^{\mathrm{T}}g + \alpha^{\mathrm{T}}p(\phi^{\mathrm{T}}W\phi). \quad (9)$$

Note that this W is defined differently to that in Dale *et al.* (2005).

Following Powell & Holland (1999), the proportions of the end-members in one independent set, p, can be converted to the proportions in another, p', with a linear transform, represented by a matrix, A

$$p = Ap' \quad \text{and} \quad p' = A^{-1}p \quad (10)$$

in which A^{-1} is the inverse of A. The transform matrix is calculated from the matrix of the mineral compositions, with each row of this composition matrix being the composition of an end-member in the independent set. If c is the composition matrix for the initial set, and c' the composition matrix corresponding to p' then A can be found from $c' = A^{\mathrm{T}}c$, in which A^{T} is the transpose of A.

In the different independent set, G^* is written in terms of p' (and ϕ), and the corresponding interaction energies, W', Gibbs energies, g', and asymmetry parameters, α', as given by an equivalent expression to Eq. (9)

$$G^* = p'^{\mathrm{T}}g' + \alpha'^{\mathrm{T}}p'(\phi'^{\mathrm{T}}W'\phi'). \quad (11)$$

Given that the right-hand sides of Eqs (9) and (11) are identically equal, the equivalences can be made. First, from the premultiplier in the second term on the right-hand sides

$$\alpha^{\mathrm{T}}p = \alpha^{\mathrm{T}}Ap' \equiv \alpha'^{\mathrm{T}}p' \quad (12)$$

so therefore $\alpha' = A^{\mathrm{T}}\alpha$ (corresponding to the relationship between c' and c). Now for ϕ. With some algebra, based on the relationship of p' to p, and α' to α

$$\phi = B\phi' \quad \text{with} \quad B = \mathrm{diag}(\alpha)A\,\mathrm{diag}(\alpha')^{-1} \quad (13)$$

in which diag converts a vector into a diagonal matrix, with the diagonal elements being the elements of the vector.

Combining Eqs (12) and (13) with Eq. (11) gives

$$G^* = p'^{\mathrm{T}}A^{\mathrm{T}}g + \alpha'^{\mathrm{T}}p'\left(\phi'^{\mathrm{T}}B^{\mathrm{T}}WB\,\phi'\right)$$
$$= p'^{\mathrm{T}}g' + \alpha'^{\mathrm{T}}p'\left(\phi'^{\mathrm{T}}Q\,\phi'\right) \quad (14)$$

in which $Q = B^{\mathrm{T}}WB$. Now the equivalences can be constructed, following Powell & Holland (1999). Comparing Eq. (14) with Eq. (9), Q will not in general be strictly upper triangular, as W is in Eq. (9), and as it needs to be, so the requirement is to convert Q to the form of Eq. (8). Some terms will end up not being able to be included in W', and these are transferred to g'. To do the conversion, Q is written as $Q_1 + Q_2 + Q_3$, in which Q_1 is that part of Q below the diagonal with the diagonal and above filled with zeroes; Q_2 is that part of Q above the diagonal with the diagonal and below filled with zeroes; and Q_3 is a diagonal matrix containing the diagonal elements of Q, the off-diagonal elements filled with zeroes. Denoting the diagonal elements by a vector, q, then $Q_3 = \mathrm{diag}(q)$. The first contributions to W' come from Q_1^{T} and Q_2. Transposing turns the strictly lower triangular matrix Q_1 into a strictly upper triangular one. Zeroing Q_3 is done by noting that the terms in Eq. (14) from Q_3 have the form $\phi_k^2 q_k$. Now $\phi_k^2 q_k$ can be written as $\phi_k(1-\sum_{j \neq k}\phi_j)q_k$. As a consequence q contributes to both g' (from terms linear in p) and w' (from terms quadratic in p). The contributions of the kth term in q are

$$\phi_k\left(1 - \sum_{j \neq k}\phi_j\right)q_k = \phi_k q_k - \sum_{j \neq k}\phi_j\phi_k q_k.$$

The first part is included in g' in the form $p'^{\mathrm{T}}Q_3\alpha$. The second part can be made to contribute to w' in the form $\phi'^{\mathrm{T}}Q_f\phi'$, with a strictly upper triangular Q_f built up from a zero matrix by adding q_k into the elements on the kth row and the kth column of the matrix, for $k = 1,2,\ldots,n$. Thus Eq. (14) becomes

$$G^* = p'^{\mathrm{T}}(A^{\mathrm{T}}g + Q_3\alpha) + \alpha'^{\mathrm{T}}p'[\phi'^{\mathrm{T}}(Q_1^{\mathrm{T}} + Q_2 + Q_f)\phi']$$
$$= p'^{\mathrm{T}}g' + \alpha'^{\mathrm{T}}p'(\phi'^{\mathrm{T}}W'\phi') \quad (15)$$

as required, with $W' = Q_1^{\mathrm{T}} + Q_2 + Q_f$ and $g' = A^{\mathrm{T}}g + Q_3\alpha$.

APPENDIX 2: RECALCULATION OF ANALYSES

Hornblende and gedrite microprobe analyses were recalculated according to the method of Holland & Blundy (1994) as outlined in Dale *et al.* (2005). However, the recalculation of cummingtonite and anthophyllite is not straightforward if octahedral site vacancies are to be avoided (Robinson *et al.*, 1982). This problem is compounded by the usual problem that ferric iron has not been analysed. Recalculation methods such as those used in Robinson *et al.* (1982) and Dale *et al.* (2005) will not work in this situation because it will give low cation totals that fail the stoichiometry criteria. Given that the A-site occupancy of these amphiboles is almost always within error of zero, the simplest assumption to make is that the cation total is 15 (on the normal 'O$_{22}$(OH)$_2$' basis), with the A-site occupancy taken to be actually zero. From an appraisal of the Rabbitt (1948) and Leake (1968) data sets, a representative conversion of FeO to Fe$_2$O$_3$ for cummingtonite and anthophyllite is 0.04.

The analyses were adjusted, in a least squares sense, using 1% relative uncertainty on the wt% oxides, such that the cation total will be 15, and that the conversion of FeO to Fe_2O_3 is 0.04. This follows the approach in Carson & Powell (1997) (used for orthopyroxene), and in Štípská & Powell (2005) (used for clinopyroxene).

APPENDIX 3: DEPENDENT END-MEMBER CONSTRAINTS ON THE EXPANSION FROM NCMASH TO NCFMASH

The full set of dependent end-member relationships for clinoamphibole in NCFMASH are given by the following, with the α values already substituted (accounting for the unusual multipliers on each W on the right-hand side of the equations):

$$W_{\text{grun fts}} = \frac{-5W_{\text{grun camo1}}}{18} + \frac{2W_{\text{ts camo1}}}{3} + \frac{W_{\text{ts grun}}}{3}$$

$$W_{\text{grun fparg}} = \frac{-135W_{\text{camo1 camo2}}}{578} - \frac{27W_{\text{grun camo1}}}{289}$$
$$- \frac{27W_{\text{grun camo2}}}{578} + \frac{10W_{\text{parg camo1}}}{17}$$
$$+ \frac{5W_{\text{parg camo2}}}{17} + \frac{2W_{\text{parg grun}}}{17}$$

$$W_{\text{grun fgl}} = \frac{5W_{\text{gl camo1}}}{4} - \frac{W_{\text{gl grun}}}{4} + \frac{9W_{\text{grun camo1}}}{32}$$

$$W_{\text{fact fts}} = \frac{-5W_{\text{camo1 camo2}}}{12} + \frac{5W_{\text{grun camo1}}}{9}$$
$$+ \frac{5W_{\text{grun camo2}}}{3} + \frac{5W_{\text{tr camo1}}}{12} + \frac{5W_{\text{tr camo2}}}{4}$$
$$- \frac{5W_{\text{tr grun}}}{3} + W_{\text{tr ts}} - \frac{W_{\text{ts camo1}}}{3}$$
$$- W_{\text{ts camo2}} + \frac{4W_{\text{ts grun}}}{3}$$

$$W_{\text{fact fparg}} = \frac{-567W_{\text{camo1 camo2}}}{1445} + \frac{3591W_{\text{grun camo1}}}{5780}$$
$$+ \frac{1539W_{\text{grun camo2}}}{1445} - \frac{7W_{\text{parg camo1}}}{17}$$
$$- \frac{12W_{\text{parg camo2}}}{17} + \frac{19W_{\text{parg grun}}}{17}$$
$$+ \frac{189W_{\text{tr camo1}}}{340} + \frac{81W_{\text{tr camo2}}}{85}$$
$$- \frac{513W_{\text{tr grun}}}{340} + W_{\text{tr parg}}$$

$$W_{\text{fact fgl}} = \frac{9W_{\text{camo1 camo2}}}{40} + \frac{W_{\text{gl camo1}}}{4} - W_{\text{gl camo2}}$$
$$+ \frac{3W_{\text{gl grun}}}{4} - \frac{27W_{\text{grun camo1}}}{160} + \frac{27W_{\text{grun camo2}}}{40}$$
$$- \frac{9W_{\text{tr camo1}}}{40} + \frac{9W_{\text{tr camo2}}}{10} + W_{\text{tr gl}}$$
$$- \frac{27W_{\text{tr grun}}}{40}$$

$$W_{\text{fts fparg}} = \frac{32W_{\text{camo1 camo2}}}{867} - \frac{352W_{\text{grun camo1}}}{13005}$$
$$+ \frac{88W_{\text{grun camo2}}}{867} - \frac{128W_{\text{parg camo1}}}{1377}$$
$$+ \frac{160W_{\text{parg camo2}}}{459} - \frac{352W_{\text{parg grun}}}{1377}$$
$$+ \frac{128W_{\text{ts camo1}}}{1275} - \frac{32W_{\text{ts camo2}}}{85}$$
$$+ \frac{352W_{\text{ts grun}}}{1275} + W_{\text{ts parg}} \tag{16}$$

$$W_{\text{fts fgl}} = \frac{161W_{\text{gl camo1}}}{216} - \frac{161W_{\text{gl grun}}}{216}$$
$$+ \frac{1127W_{\text{grun camo1}}}{2880} - \frac{161W_{\text{ts camo1}}}{300}$$
$$+ W_{\text{ts gl}} + \frac{161W_{\text{ts grun}}}{300}$$

$$W_{\text{fparg fgl}} = \frac{1125W_{\text{camo1 camo2}}}{4624} + \frac{125W_{\text{gl camo1}}}{136}$$
$$- \frac{125W_{\text{gl camo2}}}{306} - \frac{625W_{\text{gl grun}}}{1224}$$
$$+ \frac{5625W_{\text{grun camo1}}}{18496} - \frac{625W_{\text{grun camo2}}}{4624}$$
$$- \frac{125W_{\text{parg camo1}}}{204} + \frac{125W_{\text{parg camo2}}}{459}$$
$$+ W_{\text{parg gl}} + \frac{625W_{\text{parg grun}}}{1836}$$

Using the assumption that the non-ideality of the Fe subsystem amphiboles is the same as for the Mg subsystem, then all the left-hand Ws can be substituted for their Mg end-member equivalents (e.g. $W_{\text{grun fts}} = W_{\text{cumm ts}}$). Substituting the known W values at this stage of the analysis (see text), leaves the 'cross' Ws between the Mg end-members and the Fe-bearing end-members, camo1, camo2 and grun. Solving gives these in terms of one of their number (here $W_{\text{ts grun}}$):

$$W_{\text{gl camo1}} = 78.40 + 0.27W_{\text{ts grun}}$$
$$W_{\text{gl camo2}} = 24.85 + 1.08W_{\text{ts grun}}$$
$$W_{\text{gl grun}} = 5.50 + 1.35W_{\text{ts grun}}$$
$$W_{\text{parg camo1}} = 148.13 - 0.67W_{\text{ts grun}}$$
$$W_{\text{parg camo2}} = 3.28 + 1.14W_{\text{ts grun}} \tag{17}$$
$$W_{\text{parg grun}} = 68.56 + 0.48W_{\text{ts grun}}$$
$$W_{\text{ts camo1}} = 110.00 - 0.50W_{\text{ts grun}}$$
$$W_{\text{ts camo2}} = -47.50 + 1.50W_{\text{ts grun}}$$

APPENDIX 4: CODINGS FOR CLINOAMPHIBOLE AND ORTHOAMPHIBOLE

To account for all the exchange vectors in the amphibole composition and the partitioning of Fe^{2+} and Mg, eight compositional variables are required. These are defined as:

$$x = \frac{Fe^{2+}}{Fe^{2+} + Mg}\bigg|_{\text{amph}}$$
$$= \frac{(2x^{\text{M4}}_{\text{Fe2+}} + 3x^{\text{M13}}_{\text{Fe2+}} + 2x^{\text{M2}}_{\text{Fe2+}})}{(2x^{\text{M4}}_{\text{Fe2+}} + 2x^{\text{M4}}_{\text{Mg}} + 3x^{\text{M13}}_{\text{Fe2+}} + 3x^{\text{M13}}_{\text{Mg}} + 2x^{\text{M2}}_{\text{Fe2+}} + 2x^{\text{M2}}_{\text{Mg}})}$$
$$y = x^{\text{M2}}_{\text{Al}}$$
$$z = x^{\text{M4}}_{\text{Na}}$$
$$a = x^{\text{A}}_{\text{Na}}$$
$$c = x^{\text{M4}}_{\text{Ca}} \tag{18}$$
$$f = x^{\text{M2}}_{\text{Fe3+}}$$
$$Q_1 = x - \frac{x^{\text{M13}}_{\text{Fe2+}}}{x^{\text{M13}}_{\text{Fe2+}} + x^{\text{M13}}_{\text{Mg}}}$$
$$Q_2 = x - \frac{x^{\text{M2}}_{\text{Fe2+}}}{x^{\text{M2}}_{\text{Fe2+}} + x^{\text{M2}}_{\text{Mg}}}$$

From these variables, the following site fractions are derived:

$$x_v^A = 1 - a$$
$$x_{Na}^A = a$$
$$x_{Ca}^{M4} = c$$
$$x_{Na}^{M4} = z$$
$$x_{Mg}^{M4} = (1-x)(1-c-z) - Q_2(1-y-f) - \frac{3Q_1}{2}$$
$$x_{Fe}^{M4} = x(1-c-z) + Q_2(1-y-f) + \frac{3Q_1}{2}$$
$$x_{Mg}^{M13} = 1 - x + Q_1$$
$$x_{Fe}^{M13} = x - Q_1 \qquad (19)$$
$$x_{Al}^{M2} = y$$
$$x_{Fe3+}^{M2} = f$$
$$x_{Mg}^{M2} = (1 - x + Q_2)(1 - y - f)$$
$$x_{Fe2+}^{M2} = (x - Q_2)(1 - y - f)$$
$$x_{Al}^{T1} = \frac{a}{4} + \frac{f}{2} + \frac{y}{2} - \frac{z}{2}$$
$$x_{Si}^{T1} = 1 - \frac{a}{4} - \frac{f}{2} - \frac{y}{2} + \frac{z}{2}$$

The corresponding end-member proportions for clinoamphibole are:

$$tr = c + z - y - f - \frac{a}{2}$$
$$ts = y + f - z - \frac{a}{2}$$
$$parg = a$$
$$gl = z - f$$
$$cumm = (1-x)(1-c-z) - Q_2(1-y-f) - \frac{3Q_1}{2}$$
$$grun = x(1 + c + z - y - f) - 2Q_2(1-y-f) - \frac{5Q_1}{2}$$
$$camo1 = Q_2(1-y-f) - x(c+z) + \frac{5Q_1}{2}$$
$$camo2 = 2Q_2(1-y-f) - x(c+z-y-f) + \frac{3Q_1}{2} \qquad (20)$$
$$mrb = f$$

and for orthoamphibole:

$$anth = 1 - c - y - f - \frac{a}{2} - x(c+z)$$
$$\qquad\quad - Q_2(1-y-f) - \frac{3Q_1}{2}$$
$$ged = y + f - z - \frac{a}{2}$$
$$ompa = a$$
$$omgl = z - f$$
$$otr = c \qquad (21)$$
$$fanth = x(1 + c + z - y - f) - 2Q_2(1-y-f) - \frac{5Q_1}{2}$$
$$amo1 = Q_2(1-y-f) - x(c+z) + \frac{5Q_1}{2}$$
$$amo2 = 2Q_2(1-y-f) - x(c+z-y-f) + \frac{3Q_1}{2}$$
$$omrb = f$$

With the multiplicities of sites as given above, the ideal activity expressions for the clinoamphibole end-members are:

$$a_{tr} = (x_v^A)^1 (x_{Ca}^{M4})^2 (x_{Mg}^{M13})^3 (x_{Mg}^{M2})^2 (x_{Si}^{T1})^1$$
$$a_{ts} = 2(x_v^A)^1 (x_{Ca}^{M4})^2 (x_{Mg}^{M13})^3 (x_{Al}^{M2})^2 (x_{Al}^{T1})^{1/2} (x_{Si}^{T1})^{1/2}$$

$$a_{parg} = 8(x_{Na}^A)^1 (x_{Ca}^{M4})^2 (x_{Mg}^{M13})^3 (x_{Al}^{M2})^1 (x_{Mg}^{M2})^1$$
$$\qquad\qquad \times (x_{Al}^{T1})^{1/2} (x_{Si}^{T1})^{1/2}$$
$$a_{gl} = (x_v^A)^1 (x_{Na}^{M4})^2 (x_{Mg}^{M13})^3 (x_{Al}^{M2})^2 (x_{Si}^{T1})^1$$
$$a_{cumm} = (x_v^A)^1 (x_{Mg}^{M4})^2 (x_{Mg}^{M13})^3 (x_{Mg}^{M2})^2 (x_{Si}^{T1})^1 \qquad (22)$$
$$a_{grun} = (x_v^A)^1 (x_{Fe}^{M4})^2 (x_{Fe}^{M13})^3 (x_{Fe}^{M2})^2 (x_{Si}^{T1})^1$$
$$a_{camo1} = (x_v^A)^1 (x_{Fe}^{M4})^2 (x_{Mg}^{M13})^3 (x_{Fe}^{M2})^2 (x_{Si}^{T1})^1$$
$$a_{camo2} = (x_v^A)^1 (x_{Fe}^{M4})^2 (x_{Fe}^{M13})^3 (x_{Mg}^{M2})^2 (x_{Si}^{T1})^1$$
$$a_{mrb} = (x_v^A)^1 (x_{Na}^{M4})^2 (x_{Mg}^{M13})^3 (x_{Fe3+}^{M2})^2 (x_{Si}^{T1})^1$$

and for the orthoamphibole end-members:

$$a_{anth} = (x_v^A)^1 (x_{Mg}^{M4})^2 (x_{Mg}^{M13})^3 (x_{Mg}^{M2})^2 (x_{Si}^{T1})^1$$
$$a_{ged} = 2(x_v^A)^1 (x_{Mg}^{M4})^2 (x_{Mg}^{M13})^3 (x_{Al}^{M2})^2 (x_{Al}^{T1})^{1/2} (x_{Si}^{T1})^{1/2}$$
$$a_{ompa} = 8(x_{Na}^A)^1 (x_{Mg}^{M4})^2 (x_{Mg}^{M13})^3 (x_{Al}^{M2})^1 (x_{Mg}^{M2})^1 (x_{Al}^{T1})^{1/2}$$
$$\qquad\qquad \times (x_{Si}^{T1})^{1/2}$$
$$a_{omgl} = (x_v^A)^1 (x_{Mg}^{M4})^2 (x_{Mg}^{M13})^3 (x_{Al}^{M2})^2 (x_{Si}^{T1})^1 \qquad (23)$$
$$a_{otr} = (x_v^A)^1 (x_{Ca}^{M4})^2 (x_{Mg}^{M13})^3 (x_{Mg}^{M2})^2 (x_{Si}^{T1})^1$$
$$a_{fanth} = (x_v^A)^1 (x_{Fe}^{M4})^2 (x_{Fe}^{M13})^3 (x_{Fe}^{M2})^2 (x_{Si}^{T1})^1$$
$$a_{amo1} = (x_v^A)^1 (x_{Fe}^{M4})^2 (x_{Mg}^{M13})^3 (x_{Fe}^{M2})^2 (x_{Si}^{T1})^1$$
$$a_{amo2} = (x_v^A)^1 (x_{Fe}^{M4})^2 (x_{Fe}^{M13})^3 (x_{Mg}^{M2})^2 (x_{Si}^{T1})^1$$
$$a_{omrb} = (x_v^A)^1 (x_{Na}^{M4})^2 (x_{Mg}^{M13})^3 (x_{Fe3+}^{M2})^2 (x_{Si}^{T1})^1$$

The activity coefficient expression for end-member, ℓ, is

$$RT \ln \gamma_\ell = \sum_{i=1(i\neq\ell)}^{n} \phi_i (1 - \phi_\ell) W_{\ell i} \frac{2\alpha_\ell}{\alpha_\ell + \alpha_i}$$
$$\qquad - \sum_{i=1(i\neq\ell)}^{n-1} \sum_{j=i+1(j\neq\ell)}^{n} \phi_i \phi_j W_{\ell i} \frac{2\alpha_\ell}{\alpha_i + \alpha_j} \qquad (24)$$

So, for example for the end-member tremolite in clinoamphibole,

$$RT \ln \gamma_{tr} = \sum_{i=1(i\neq tr)}^{n} \phi_i (1 - \phi_{tr}) W_{tri} \frac{2\alpha_{tr}}{\alpha_{tr} + \alpha_i}$$
$$\qquad - \sum_{i=1(i\neq tr)}^{n-1} \sum_{j=i+1(j\neq tr)}^{n} \phi_i \phi_j W_{tri} \frac{2\alpha_{tr}}{\alpha_i + \alpha_j} \qquad (25)$$

In these, n is the number of end-members in the independent set used to represent the thermodynamics, so for the full system, NCFMASHO, $n = 9$. The ϕ are defined as

$$\phi_k = \frac{\alpha_k p_k}{\sum_{i=1}^{n} \alpha_i p_i} \qquad (26)$$

As in the text, p_i is the proportion of end-member i, α_i is the asymmetry parameter for end-member i, and W_{ij} is the (macroscopic) interaction energy between end-members i and j.

To show an activity coefficient without using $\sum$, the following is the activity coefficient for tremolite in the $n = 4$ NCMASH system

$$RT \ln \gamma_{tr} = \phi_{ts}(1 - \phi_{tr}) W_{tr\,ts} \frac{2\alpha_{tr}}{\alpha_{tr} + \alpha_{ts}}$$
$$\qquad + \phi_{parg}(1 - \phi_{tr}) W_{tr\,parg} \frac{2\alpha_{tr}}{\alpha_{tr} + \alpha_{parg}}$$
$$\qquad + \phi_{gl}(1 - \phi_{tr}) W_{tr\,gl} \frac{2\alpha_{tr}}{\alpha_{tr} + \alpha_{gl}} - \phi_{ts}\phi_{parg}$$
$$\qquad \times W_{ts\,parg} \frac{2\alpha_{tr}}{\alpha_{ts} + \alpha_{parg}} - \phi_{ts}\phi_{gl} W_{ts\,gl} \frac{2\alpha_{tr}}{\alpha_{ts} + \alpha_{gl}}$$
$$\qquad - \phi_{parg}\phi_{gl} W_{parg\,gl} \frac{2\alpha_{tr}}{\alpha_{parg} + \alpha_{gl}}$$

with for example

$$\phi_{parg} = \frac{\alpha_{parg}p_{parg}}{\alpha_{tr}p_{tr} + \alpha_{ts}p_{ts} + \alpha_{parg}p_{parg} + \alpha_{gl}p_{gl}}$$

As can be seen in this example, for a system with $n = 4$, there are six terms. In a n end-member system there are $\frac{1}{2}n(n - 1)$ terms. So for $n = 9$, there are 36 terms.

Models such as this one for amphibole, with many terms and moreover involving order–disorder so that internal equilibria are involved, cannot be easily handled without appropriate software. THERMOCALC (Powell & Holland, 1988), used above to calculate the phase diagrams, can also be used to calculate the activities of the amphibole end-members for specified amphibole composition at given P–T (using mode 2). Mode 0 can be used to generate a table of end-member properties. Both of these require the appropriate THERMOCALC datafile coding (available from the authors or at http://www.earthsci.unimelb.edu.au/tpg/thermocalc/).